LETTER

https://doi.org/10.1038/s41586-019-1112-8

p38γ is essential for cell cycle progression and liver tumorigenesis

Antonia Tomás-Loba[1], Elisa Manieri[1,2,19], Bárbara González-Terán[1,19], Alfonso Mora[1], Luis Leiva-Vega[1], Ayelén M. Santamans[1], Rafael Romero-Becerra[1], Elena Rodríguez[1], Aránzazu Pintor-Chocano[1], Ferran Feixas[3], Juan Antonio López[1], Beatriz Caballero[1], Marianna Trakala[4], Óscar Blanco[5], Jorge L. Torres[5], Lourdes Hernández-Cosido[5], Valle Montalvo-Romeral[1], Nuria Matesanz[1], Marta Roche-Molina[1], Juan Antonio Bernal[1], Hannah Mischo[6], Marta León[1], Ainoa Caballero[1], Diego Miranda-Saavedra[7,8], Jesús Ruiz-Cabello[1,9,10,11,13], Yulia A. Nevzorova[12,13], Francisco Javier Cubero[14,15], Jerónimo Bravo[16], Jesús Vázquez[1,17], Marcos Malumbres[4], Miguel Marcos[5], Sílvia Osuna[3,18] & Guadalupe Sabio[1]*

The cell cycle is a tightly regulated process that is controlled by the conserved cyclin-dependent kinase (CDK)–cyclin protein complex[1]. However, control of the G0-to-G1 transition is not completely understood. Here we demonstrate that p38 MAPK gamma (p38γ) acts as a CDK-like kinase and thus cooperates with CDKs, regulating entry into the cell cycle. p38γ shares high sequence homology, inhibition sensitivity and substrate specificity with CDK family members. In mouse hepatocytes, p38γ induces proliferation after partial hepatectomy by promoting the phosphorylation of retinoblastoma tumour suppressor protein at known CDK target residues. Lack of p38γ or treatment with the p38γ inhibitor pirfenidone protects against the chemically induced formation of liver tumours. Furthermore, biopsies of human hepatocellular carcinoma show high expression of p38γ, suggesting that p38γ could be a therapeutic target in the treatment of this disease.

Despite the identified role of CDKs in cell cycle progression, the precise molecular mechanisms that trigger initiation of the cell cycle are unknown in most cell types. The p38 MAPKs (p38α, p38β, p38γ and p38δ) and the CDKs belong to the CMGC protein kinase superfamily[2]. Sequence analysis of the catalytic domains of proteins from this superfamily showed that the p38 MAPKs form a sister group within the CDK family (Extended Data Fig. 1a). A heuristic three-dimensional (3D) search of active CDK1 and CDK2 revealed a higher degree of structural similarity with p38γ than with other stress kinases (Supplementary Table 1). Molecular dynamics simulations showed that the CDK1 inhibitor RO3306 has a similar affinity for the ATP-binding site of p38γ as it does for CDK1; it has weaker affinities for CDK2 and p38δ, and no affinity towards p38α. This suggests that p38γ and CDK1 have similar inhibition mechanisms (Extended Data Fig. 1b–e, Supplementary Videos 1, 2).

To test whether p38γ and CDKs share common substrates, we studied retinoblastoma tumour suppressor protein (Rb). Rb remains hypophosphorylated and active in G0, but during cell cycle progression it is sequentially phosphorylated by CDKs; its subsequent inactivation promotes entry into the cell cycle and proliferation[3]. In vitro kinase assays revealed that p38γ equally phosphorylated Rb at 12 CDK target residues[3] (Extended Data Figs. 1f, 2a). Moreover, we detected Rb in immunoprecipitates of p38γ from liver lysates (Fig. 1a). p38γ-mediated Rb phosphorylation in vivo was confirmed in livers from p38γ-knockout (*Mapk12*$^{-/-}$) mice that were infected with liver-specific adeno-associated viruses expressing a constitutively active form of p38γ (AAVp38γ*) (Fig. 1b). These data indicate that p38γ has

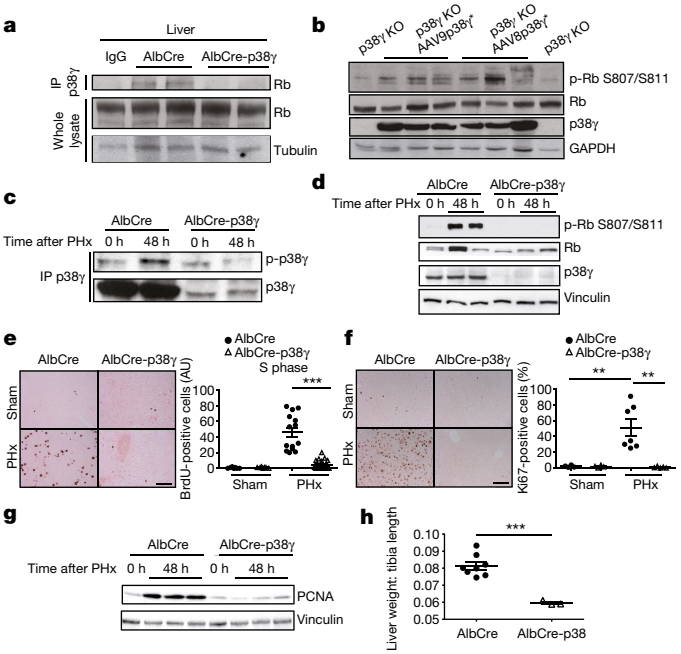

Fig. 1 | p38γ phosphorylates Rb and promotes liver proliferation after PHx. a, Immunoprecipitation from control livers (AlbCre mice, using IgG) and from livers in which p38γ was specifically knocked out (AlbCre-p38γ mice, using anti-p38γ), after treatment with DEN for 48 h. **b**, Immunoblots from livers of p38γ-knockout (p38γ KO) mice injected with adeno-associated virus (AAV8 or AAV9) expressing active p38γ (p38γ*). The prefix 'p-' indicates phosphorylation. **c**–**g**, Analysis of livers from AlbCre and AlbCre-p38γ mice 48 h after PHx or sham procedure. **c**, **d**, Liver immunoblot. **e**, BrdU immunostaining. Left, representative images; right, quantification of BrdU-positive cells. $n = 3$–7. **f**, Ki67 immunostaining. Left, representative images; right, quantification of Ki67-positive cells. $n = 4$–6. **g**, Proliferating cell nuclear antigen (PCNA) immunoblot. **h**, Ratio of liver weight (g) to tibia length (mm), 15 days after surgery. $n = 3$–8. All quantifications are shown as mean ± s.e.m. Comparisons were made by one-way analysis of variance (ANOVA) coupled to Bonferroni's post-test (**e**, **f**) or two-sided Student's *t*-test (**h**); $^{**}P < 0.01$; $^{***}P < 0.001$. Scale bars, 100 μm.

[1]Centro Nacional de Investigaciones Cardiovasculares (CNIC), Madrid, Spain. [2]Centro Nacional de Biotecnología, CSIC, Madrid, Spain. [3]Departament de Química and Institut de Química Computacional i Catàlisi, Universitat de Girona, Girona, Spain. [4]Centro Nacional de Investigaciones Oncológicas (CNIO), Madrid, Spain. [5]University of Salamanca, University Hospital of Salamanca-IBSAL, Salamanca, Spain. [6]Sir William Dunn School of Pathology, Oxford University, Oxford, UK. [7]Centro de Biología Molecular Severo Ochoa, CSIC/Universidad Autónoma de Madrid, Madrid, Spain. [8]University of Oxford Wolfson Building, Oxford, UK. [9]CIC biomaGUNE, 2014, Donostia-San Sebastián, Spain. [10]IKERBASQUE, Basque Foundation for Science, Bilbao, Spain. [11]Ciber de Enfermedades Respiratorias (CIBERES), Madrid, Spain. [12]University Hospital RWTH Aachen, Aachen, Germany. [13]Faculty of Biology, Complutense University, Madrid, Spain. [14]Complutense University School of Medicine, Madrid, Spain. [15]12 de Octubre Health Research Institute (imas12), Madrid, Spain. [16]Instituto de Biomedicina de Valencia, IBV-CSIC, Valencia, Spain. [17]CIBER Enfermedades Cardiovasculares (CIBERCV), Madrid, Spain. [18]ICREA, Barcelona, Spain. [19]These authors contributed equally: Elisa Manieri, Bárbara González-Terán. *e-mail: gsabio@cnic.es

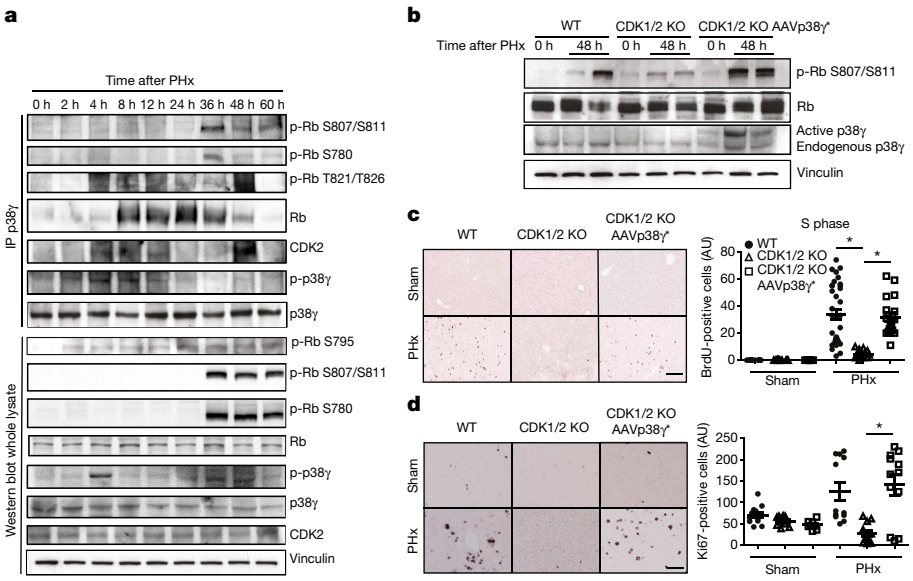

Fig. 2 | p38γ compensates for the loss of CDK1 or CDK2. a, Immunoprecipitation (using anti-p38γ) from liver lysates of wild-type mice that were euthanized at the indicated time points after PHx. **b**–**d**, Analysis of livers from wild-type mice (WT), CDK1/2 knockout (AAV2/8-Cre) mice (CDK1/2 KO) and CDK1/2 knockout mice infected with active p38γ (CDK1/2 KO AAVp38γ*) after PHx or sham procedure. **b**, Liver immunoblot. **c**, BrdU immunostaining. Left, representative images; right, quantification of BrdU-positive cells. AU, arbitrary units. $n = 4$–7. **d**, Ki67 immunostaining. Left, representative images; right, quantification of Ki67-positive cells. One-way ANOVA coupled to Kruskal–Wallis post-tests (**c**, **d**); $^*P < 0.05$. Scale bars, 500 μm. All quantifications are shown as mean ± s.e.m.

similarities with CDKs: it shares structural homology, comparable binding dynamics for RO3306 in the ATP-binding site and a similar substrate specificity.

Phosphorylation-induced Rb inactivation in hepatocytes is sufficient to promote the G0-to-G1 transition[4,5]. After partial hepatectomy (PHx)—a well-established model of hepatocyte proliferation—p38γ was phosphorylated and activated (Fig. 1c). To address the physiological effect of p38γ-mediated Rb phosphorylation after PHx, we compared hepatocyte proliferation in mice that lacked p38γ in hepatocytes (AlbCre-p38γ) and in control AlbCre mice (AlbCre$^{+/-}$). Whereas PHx induced the phosphorylation of Rb in control mice, this effect was abolished in AlbCre-p38γ mice (Fig. 1d) without changes in CDK expression (Extended Data Fig. 2b). Loss of Rb phosphorylation in AlbCre-p38γ mice correlated with reduced induction of cyclin E and A (Extended Data Fig. 2b). Compared with AlbCre mice, AlbCre-p38γ mice also showed markedly reduced hepatic DNA synthesis and hepatocyte proliferation—as measured by bromodeoxyuridine (BrdU) incorporation, Ki67 immunostaining and proliferating cell nuclear antigen expression (Fig. 1e–g). The reduced hepatocyte proliferation in AlbCre-p38γ mice was reflected in a reduced extent of liver regeneration (Fig. 1h, Extended Data Fig. 3a). Together, these results indicate that p38γ is required in hepatocytes for Rb phosphorylation and liver regeneration.

To corroborate these results and avoid the effects of unspecific deletion of p38γ, we infected AlbCre-p38γ mice with AAVp38γ*. The hepatocyte-specific expression of active p38γ recovered hepatocyte proliferation, Rb phosphorylation and liver regeneration (Extended Data Fig. 3b–f). It is known that N-terminal Rb phosphorylation by p38α delays cell cycle progression, rendering Rb insensitive to regulation by CDKs[6]. However, unlike hepatocyte-specific active p38α, active p38γ promoted phosphorylation of the Rb C terminus and hepatocyte proliferation (Extended Data Fig. 3g, h).

Lack of p38γ was found to impair liver regeneration, although it did not affect survival (Extended Data Fig. 4a). This is consistent with peak Rb phosphorylation and hepatocyte proliferation, which occurred at 60 h after PHx (Extended Data Fig. 4b, f). p38δ—the p38 isoform that is most closely related to p38γ—can compensate for the lack of p38γ and can phosphorylate its substrates[7–9]. The expression of p38δ

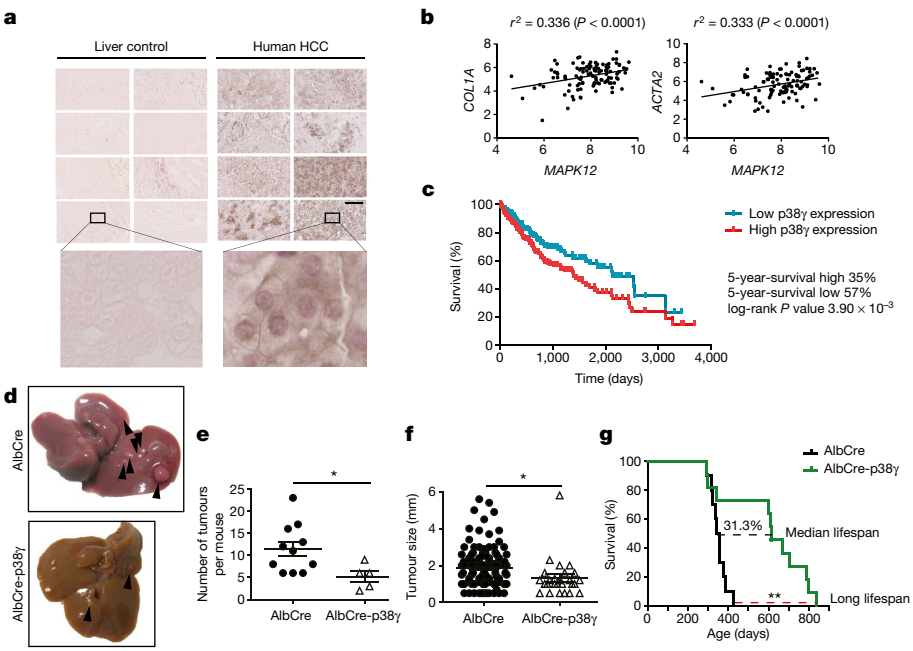

Fig. 3 | p38γ drives the development of HCC. a, p38γ immunostaining in human HCC and healthy liver control. Scale bar, 500 μm. **b**, Pearson's correlation of mRNA levels in human livers, comparing expression levels of *MAPK12* with those of *COL1A* (encoding collagen, left) and *ACTA2* (encoding actin, right). $n = 107$. **c**, Kaplan–Meier survival curves of patients stratified by p38γ expression. $n = 372$. **d**–**f**, Analysis of DEN-induced HCC in six-month-old AlbCre and AlbCre-p38γ mice. **d**, Photographs of livers from an AlbCre mouse (top) and an AlbCre-p38γ mouse (bottom). Arrows mark tumours. **e**, **f**, Number of tumours (**e**) and tumour size (**f**) in AlbCre and AlbCre-p38γ mice. $n = 5$–11. $^*P < 0.05$. **g**, Kaplan–Meier analysis of survival. $n = 10, 11$. $^{**}P < 0.01$. Scale bar, 100 μm. 31.3% is the difference in median lifespan between AlbCre and AlbCre-p38γ mice. All quantifications are shown as mean ± s.e.m. Comparisons were performed using a Mantel–Cox log-rank test (**c**, **g**); Mann–Whitney *U*-test (**e**); or two-sided Student's *t*-test (**f**).

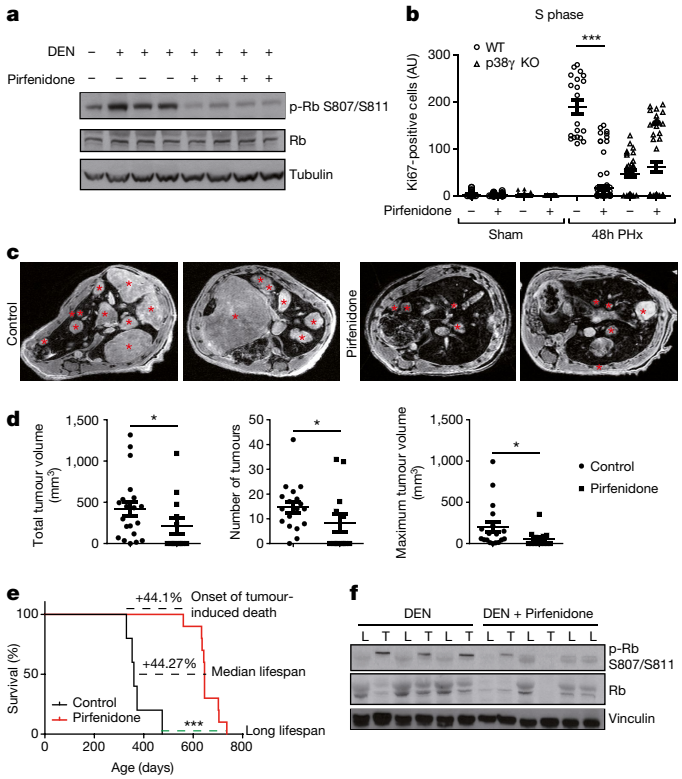

Fig. 4 | Pirfenidone inhibits p38γ activity and protects against DEN-induced HCC. a, Immunoblot of mouse liver 2 weeks after acute treatment with DEN. **b**, Ki67 immunohistochemistry in pirfenidone-treated mice before PHx. $n = 5$–17. One-way ANOVA; $^{***}P < 0.001$. **c**–**e**, Livers were imaged 11 months after DEN injection, with or without pirfenidone treatment. **c**, MRI scans of control and pirfenidone-treated livers. **d**, Number of tumours, maximum tumour volume and total tumour volume per mouse ($n = 20$–13), analysed from magnetic resonance images using OsiriX software; Mann–Whitney *U*-test; $^{*}P < 0.05$. **e**, Kaplan–Meier analysis of survival. The percentages are the differences in onset of tumour-induced death and median lifespan between control and pifenidone-treated mice. $n = 9$–6. Mantel–Cox log-rank test; $^{***}P < 0.001$. **f**, Immunoblot analysis in hepatic tumours (T) and lesion-free peritumour zones (L) in mice treated as in **d**–**f**. All data are mean ± s.e.m.

in AlbCre-p38γ mice increased after PHx (Extended Data Fig. 4c), and in hepatocytes that lacked both kinases (AlbCre-p38γδ), Rb phosphorylation was abolished and hepatocyte proliferation was significantly delayed (Extended Data Fig. 4d–h). Furthermore, stress-activated p38γ-mediated cell cycle regulation is not restricted to hepatocytes, because p38γ was also found to phosphorylate Rb in gut epithelial cells that were treated with dextran sodium sulfate (Extended Data Fig. 5).

The precise mechanism by which Rb is phosphorylated in vivo remains unclear, because single genetic ablation of CDK2 or CDK1 does not block hepatocyte DNA replication during liver regeneration[10,11]. In vitro kinase assays with CDK2 and p38γ* showed that a greater number of Rb residues were phosphorylated when both kinases were used, which suggests that these kinases work together to control Rb phosphorylation (Extended Data Fig. 6a). Immunoprecipitation analysis confirmed a binding interaction between p38γ and CDK2 in hepatocytes (Extended Data Fig. 6b, c). To explore the cooperation between p38γ and CDK2, we examined the activation of these kinases after PHx by western blot. p38γ was activated just 4 h after PHx, as evidenced by its increased binding of Rb and by Rb phosphorylation at Ser795, Ser821 and Ser826. Moreover, a second p38γ activation peak was detected at 24 h—corresponding to the phosphorylation of Rb on residues Ser807, Ser811 and Ser780—followed by hepatocyte proliferation as detected by BrdU incorporation (Fig. 2a, Extended Data Fig. 6d). Interaction between CDK2 and p38γ increased during these two p38γ activation peaks (Fig. 2a). These results correlate with a stronger interaction between CDK2 and Rb when p38γ is present (Extended Data Fig. 6e), whereas p38γ binding to Rb was shown to be independent of CDK1 and CDK2 (Extended Data Fig. 6c). Moreover, studies with a nonphosphorylatable Rb mutant[12] indicated that the phosphorylation of Rb is required in order for it to bind to CDK2 (Extended Data Fig. 6f).

In addition, p38γ was able to compensate for the loss of CDK1 or CDK2. Infection with AAVp38γ* rescued Rb phosphorylation after silencing or ablation of the genes that encode CDK1 or CDK2, and fully preserved hepatocyte proliferation and hepatic DNA synthesis in the livers of CDK1- or CDK2-depleted mice (Fig. 2b–d, Extended Data Fig. 6g–i). Collectively, these results suggest that p38γ controls hepatocyte proliferation through the regulation of Rb phosphorylation, and probably induces proliferation through cooperation with classical CDKs. Moreover, infection with AAVp38γ* rescued Rb phosphorylation and proliferation after silencing of the genes that encode CDK4 and CDK6 (Extended Data Fig. 6j–m); this confirms the ability of p38γ to phosphorylate Rb in the absence of these CDKs.

CDK1 ablation is known to protect against liver tumorigenesis[13]. Notably, the mutation rates of CDK1 and p38γ in human hepatocellular carcinoma (HCC) samples are similar (Extended Data Fig. 7a), and the mutations located in the L16 loop of p38γ induce its activation[14]. p38γ expression was also found to be higher in human HCC cell lines than in primary hepatocytes (Extended Data Fig. 7b), and p38γ was activated in livers from genetically engineered HCC mouse models (Extended Data Fig. 7c). Furthermore, p38γ staining was far stronger in human HCC biopsies than in non-tumour tissues (Fig. 3a, Extended Data Fig. 7d). *MAPK12* expression directly correlated with the expression of *ACTA2* and *COL1A*; these genes encode actin and collagen, respectively, which are markers of fibrosis that usually precede the development of liver cancer (Fig. 3b, Supplementary Table 2). Moreover, high p38γ expression was associated with a poorer outcome in cases of liver cancer (Fig. 3c), and p38γ knockdown attenuated proliferation and colony formation in HCC cell lines (Extended Data Fig. 8). These findings may indicate an involvement of p38γ in the development of human liver tumours.

In agreement, p38γ was activated after the injection of diethylnitrosamine (DEN), and p38γ deficiency markedly attenuated DEN-induced Rb phosphorylation and compensatory proliferation, correlating with reduced expression of proliferating cell nuclear antigen and reduced proliferation of hepatocytes (Extended Data Fig. 9a–c). Moreover, HCC was strongly suppressed in AlbCre-p38γ mice, which had smaller and fewer tumours and improved survival times compared with AlbCre mice (Fig. 3d–g).

AlbCre-p38γ mice were also protected against liver cancer induced by carbon tetrachloride or by in combination with a high-fat diet (Extended Data Fig. 9d–g). We next evaluated the effect of p38γ inactivation on liver tumorigenesis. The inhibitor pirfenidone bound to and inhibited p38γ without affecting CDK2 activity (Fig. 4a, Extended Data Fig. 10a, b), and reduced hepatic DNA synthesis in wild-type mice but not in AlbCre-p38γ mice, indicating a p38γ-mediated effect (Fig. 4b). Pirfenidone reduced the number and size of liver tumours in DEN-treated mice and improved their survival, without evident secondary effects (Fig. 4c–e, Extended Data Fig. 10c). Moreover, the therapeutic effects of p38γ inhibition were confirmed by the specific ablation of p38γ using AAV2/8-CAG-Cre once the tumours were already established (Extended Data Fig. 10d–g). Notably, the tumours that grew in the pirfenidone-treated mice lost Rb expression (Fig. 4f); this suggests that, upon pirfenidone treatment, only tumours that lack Rb are able to proliferate. These data are consistent with the inactivation of tumour suppressors such as Rb through chromosomal mutations during tumour development[15], thus indicating that pirfenidone could be effective against HCC tumours that maintain Rb expression.

Our results show that p38γ functions in collaboration with CDK; this is similar to the role of MAPK in CDK signalling that has recently been established in yeast[16]. Members of the p38 MAPK protein family

can be grouped into two classes, with p38α and p38β in one class, and p38γ and p38δ in the other[17]. All members of this family share the same mechanism of activation by upstream MAPK kinases; however, the two classes do not share substrate specificity or inhibitor selectivity. p38α increases cell survival by N-terminal phosphorylation of Rb, which renders Rb insensitive to inactivation by CDKs[6]. Consequently, the knockdown of p38α in hepatocytes results in increased development of HCC[18]. These results reinforce the idea that different p38 isoforms can have opposing functions[19].

We have demonstrated that p38γ is sufficient to induce entry into the cell cycle even when the expression of CDKs is downregulated. This might allow for a cell cycle regulation that is different from the canonical mitogenic signal and CDK activation pathway, and instead functions via stress damage and p38γ activation, thereby exerting a tight regulation on the cell cycle.

This study suggests that a non-classical CDK could initiate the cell cycle in a cyclin-independent manner in quiescence, when CDK–cyclin complexes are less abundant. p38γ may represent a unique type of kinase that enables cells to escape from quiescence in response to stress stimuli. The confirmation that p38γ is essential for Rb-dependent cell cycle progression and liver tumorigenesis strongly supports the potential of p38γ as a therapeutic target in HCC, and could provide a new approach towards the treatment of this disease.

Online content

Any methods, additional references, Nature Research reporting summaries, source data, statements of data availability and associated accession codes are available at https://doi.org/10.1038/s41586-019-1112-8.

Received: 11 October 2017; Accepted: 7 March 2019;
Published online: 10 April 2019

1. Malumbres, M. Cyclin-dependent kinases. *Genome Biol.* **15**, 122 (2014).
2. Varjosalo, M. et al. The protein interaction landscape of the human CMGC kinase group. *Cell Rep.* **3**, 1306–1320 (2013).
3. Malumbres, M. & Barbacid, M. Cell cycle, CDKs and cancer: a changing paradigm. *Nat. Rev. Cancer* **9**, 153–166 (2009).
4. Canhoto, A. J., Chestukhin, A., Litovchick, L. & DeCaprio, J. A. Phosphorylation of the retinoblastoma-related protein p130 in growth-arrested cells. *Oncogene* **19**, 5116–5122 (2000).
5. Mayhew, C. N. et al. Liver-specific pRB loss results in ectopic cell cycle entry and aberrant ploidy. *Cancer Res.* **65**, 4568–4577 (2005).
6. Gubern, A. et al. The N-terminal phosphorylation of RB by p38 bypasses its inactivation by CDKs and prevents proliferation in cancer cells. *Mol. Cell* **64**, 25–36 (2016).
7. Sabio, G. et al. p38γ regulates the localisation of SAP97 in the cytoskeleton by modulating its interaction with GKAP. *EMBO J.* **24**, 1134–1145 (2005).
8. González-Terán, B. et al. p38γ and δ promote heart hypertrophy by targeting the mTOR-inhibitory protein DEPTOR for degradation. *Nat. Commun.* **7**, 10477 (2016).
9. González-Terán, B. et al. Eukaryotic elongation factor 2 controls TNF-α translation in LPS-induced hepatitis. *J. Clin. Invest.* **123**, 164–178 (2013).
10. Lundberg, A. S. & Weinberg, R. A. Functional inactivation of the retinoblastoma protein requires sequential modification by at least two distinct cyclin-cdk complexes. *Mol. Cell. Biol.* **18**, 753–761 (1998).
11. Hu, W. et al. Concurrent deletion of cyclin E1 and cyclin-dependent kinase 2 in hepatocytes inhibits DNA replication and liver regeneration in mice. *Hepatology* **59**, 651–660 (2014).
12. Narasimha, A. M. et al. Cyclin D activates the Rb tumor suppressor by mono-phosphorylation. *eLife* **3**, e02872 (2014).
13. Diril, M. K. et al. Cyclin-dependent kinase 1 (Cdk1) is essential for cell division and suppression of DNA re-replication but not for liver regeneration. *Proc. Natl Acad. Sci. USA* **109**, 3826–3831 (2012).
14. Diskin, R., Askari, N., Capone, R., Engelberg, D. & Livnah, O. Active mutants of the human p38α mitogen-activated protein kinase. *J. Biol. Chem.* **279**, 47040–47049 (2004).
15. Giacinti, C. & Giordano, A. RB and cell cycle progression. *Oncogene* **25**, 5220–5227 (2006).
16. Repetto, M. V. et al. CDK and MAPK synergistically regulate signaling dynamics via a shared multi-site phosphorylation region on the scaffold protein Ste5. *Mol. Cell* **69**, 938–952.e6 (2018).
17. Manieri, E. & Sabio, G. Stress kinases in the modulation of metabolism and energy balance. *J. Mol. Endocrinol.* **55**, R11–R22 (2015).
18. Hui, L. et al. p38α suppresses normal and cancer cell proliferation by antagonizing the JNK-c-Jun pathway. *Nat. Genet.* **39**, 741–749 (2007).
19. Matesanz, N. et al. p38α blocks brown adipose tissue thermogenesis through p38δ inhibition. *PLoS Biol.* **16**, e2004455 (2018).

Acknowledgements We thank S. Bartlett for English editing, D. Engelberg for the constitutively active mutants, the Division of Signal Transduction Therapy for recombinant proteins, and CNIC Advanced Imaging and Vector Units for technical support. G.S. (RYC-2009-04972), F.J.C. (RYC-2014-15242), and Y.A.N. (RYC-2015-17438) are investigators of the Ramón y Cajal Program. E.M. and M.T. were awarded La Caixa fellowships and R.R.-B. was a fellow of the Fundación Ramón Areces-UAM and FPU. B.G.-T. is a fellow of the FPI Severo Ochoa CNIC program (SVP-2013-067639). F.J.C. is a Gilead Liver Research Scholar. This work was funded by grants supported in part by funds from the European Regional Development Fund: the European Union's Seventh Framework Programme (FP7/2007-2013) ERC 260464, EFSD/Lilly European Diabetes Research Programme Dr Sabio, 2017 Leonardo Grant for Researchers and Cultural Creators, BBVA Foundation (Investigadores-BBVA-2017) IN[17]_BBM_BAS_0066, MINECO-FEDER SAF2016-79126-R, and Comunidad de Madrid IMMUNOTHERCAN-CM S2010/BMD-2326 and B2017/BMD-3733 to G.S.; Juan de la Cierva and MINECO SAF2014-61233-JIN to A.T.-L.; the European Community for MSCA-IF-2014-EF-661160-MetAccembly grant to F.F.; Spanish MINECO CTQ2014-59212-P, European Community for CIG project (PCIG14-GA-2013-630978), and European Research Council (ERC) under the European Union's Horizon 2020 (ERC-2015-StG-679001-NetMoDEzyme) to S.O.; the German Research Foundation (SFB/TRR57/P04 and DFG NE 2128/2-1) and MINECO SAF2017-87919R to Y.A.N.; EXOHEP-CM S2017/BMD-3727 and the COST Action CA17112, MINECO SAF2016-78711, and the AMMF Cholangiocarcinoma Charity 2018/117 to F.J.C.; MINECO (SAF2015-69920-R co-funded by ERDF-EU), the Consolider-Ingenio 2010 Programme (SAF2014-57791-REDC), Excellence Network CellSYS (BFU2014-52125-REDT), and the iLUNG Programme (B2017/BMD-3884) from the Comunidad de Madrid to M. Malumbres; MINECO SAF2015-67077-R and SAF2017-89901-R to J.B.; MINECO (BIO2015-67580-P), Carlos III Institute of Health-Fondo de Investigación Sanitaria (ProteoRed PRB3, IPT17/0019 - ISCIII-SGEFI/ERDF), Fundación La Marató and 'La Caixa' Banking Foundation (HR17-00247) to J.V.; ISCIII and FEDER PI16/01548 and Junta de Castilla y León GRS 1362/A/16 and INT/M/17/17 to M. Marcos; Junta de Castilla y León GRS 1356/A/16 and GRS 1587/A/17 to J.L.-T.; and MCNU (SAF2017-84494-C2-1-R) to J.R.-C. The CNIC is supported by the Ministerio de Ciencia, Innovación y Universidades (MCNU) and the Pro CNIC Foundation, and is a Severo Ochoa Center of Excellence (SEV-2015-0505).

Author contributions G.S. conceived and supervised this project. G.S. and A.T.-L. designed and developed the hypothesis. E.M., L.L.-V., M.L. and A.T.-L. performed experiments using DEN, carbon tetrachloride, streptozotocin and dextran sodium sulfate, and A.T.-L. analysed the data. B.G.-T., A.T.-L. and A.M. performed partial hepatectomies. A.M., A.M.S., R.R.-B. and A.T.-L. prepared Fig. 2a. A.T.-L., H.M. and B.C. performed cell experiments. A.P.-C. performed S10b. E.R., A.P.-C. and A.C. carried out immunostaining experiments and A.T.-L. analysed the data. M. Malumbres, M.T., A.M., A.M.S., V.M.-R. and A.T.-L. performed CDK1/2 knockout experiments and immunohistochemistry. M. Marcos, L.H.-C., O.B., J.L.T. and N.M. performed the analysis of human samples. Y.A.N., F.J.C. and R.R.-B. developed genetic HCC models. S.O. and F.F. carried out molecular dynamics simulations. J.A.B. and M.R.-M. generated the AAVs. J.B. performed heuristic three-dimensional analysis. J.A.L. and J.V. performed and analysed the proteomic experiments. J.R.-C. carried out MRI experiments and A.T.-L. analysed the data. D.M.-S. generated the phylogenetic tree. A.T.-L. performed the remainder of the experiments. A.T.-L. and G.S. wrote the manuscript with input from all authors.

Competing interests The authors declare no competing interests.

Additional information
Extended data is available for this paper at https://doi.org/10.1038/s41586-019-1112-8.
Supplementary information is available for this paper at https://doi.org/10.1038/s41586-019-1112-8.
Reprints and permissions information is available at http://www.nature.com/reprints.
Correspondence and requests for materials should be addressed to G.S.
Publisher's note: Springer Nature remains neutral with regard to jurisdictional claims in published maps and institutional affiliations.

METHODS

Study population and sample collection. Immunohistochemical staining of p38γ was performed in liver samples from 46 patients (86.1% male, mean age 69.2 years, standard deviation (s.d.) 22.6 years) and 11 controls (36.4% male, mean age 45.9 years, s.d. 14.7 years) recruited at the University Hospital of Salamanca, Spain. Patients were diagnosed with hepatocellular carcinoma by liver biopsy, and control individuals were recruited from patients who underwent laparoscopic cholecystectomy for gallstone disease and had no laboratory or histopathological evidence of other liver diseases. This study was approved by the Ethics Committee of the University Hospital of Salamanca. Need for informed consent for immunostaining analysis from stored tissue from patients with liver cancer was waived by the Ethical Committee. A portion of each liver biopsy was fixed in 10% formalin and stained with haematoxylin and eosin (H&E) and Masson's trichrome for standard histopathological interpretation. Immunostaining of p38γ was performed with an antibody from R&D (AF1347; 1:250).

For the analysis of liver mRNA levels, the study population included two groups. One group consisted of obese adult patients with body mass index (BMI) ≥ 35 kg m^{-2} and a liver biopsy compatible with non-alcoholic fatty liver disease who underwent elective bariatric surgery ($n = 79$). The second group consisted of individuals with BMI < 35 kg m^{-2} who underwent laparoscopic cholecystectomy for cholelithiasis ($n = 30$). Participants were excluded if they had a history of alcohol use disorders or excessive alcohol consumption (>30 g per day in men and >20 g per day in women), chronic hepatitis C or B, or if laboratory and/or histopathological data showed causes of liver disease other than non-alcoholic fatty liver disease. The study was approved by the Ethics Committee of the University Hospital of Salamanca and all subjects provided written informed consent to undergo liver biopsy under direct vision during surgery. All patients signed written informed consent for participation. Data were collected on demographic information (age, sex and ethnicity), anthropomorphic measurements (BMI), smoking and alcohol history, coexisting medical conditions and medication use. Before surgery, fasting venous blood samples were collected for determination of complete blood cell count, total bilirubin, aspartate aminotransferase, alanine aminotransferase, total cholesterol, high-density lipoprotein, low-density lipoprotein, triglycerides, creatinine, glucose and albumin. Baseline characteristics of these groups are listed in Supplementary Table 2. Kaplan–Meier survival curves of patients stratified by low or high expression of p38γ were obtained and plotted from the Human Protein Atlas database.

Animal maintenance and treatments. Mice were housed in a pathogen-free animal facility under a 12 h light/dark cycle at constant temperature and humidity, and fed standard rodent chow and water ad libitum. For all studies, we used p38γloxP (B6.129-Mapk12tm1), p38δloxP (B6.129-Mapk13tm1)[20], AlbCre (B6.Cg-Tg(Albcre)21Mgn/J)[21] and whole-body knockout mice for p38γ. Mice were backcrossed for at least 10 generations in C57BL/6. Cdk1-lox; Cdk2-knockout mice, cMYCtg and LIKKγ knockout were described previously[22–24]. Genotypes were determined by PCR. All experiments were performed with male mice. Experiments involving animals were conducted in accordance with the Guide for the Care and Use of Laboratory Animals and approved by the CNIC Animal Care and Use Committee. The maximum tumour size permitted was 15 mm.

For long-term studies of liver tumour development and Kaplan–Meier analysis different protocols were assessed: (i) 15-day-old mice received a single intraperitoneal (i.p.) injection of diethylnitrosamine (DEN; Sigma-Aldrich) dissolved in saline at a dose of 50 mg kg^{-1} body weight. Pirfenidone (CAS: 53179-13-8; eBioChem) was administrated in drinking water at 2 g l^{-1} starting at 7 months after DEN injection and continuing for 3 months. Mice in one randomly pre-assigned group were euthanized at 1 or 6 months after DEN administration for histological and biochemical analyses. Age-matched mice in a second group were used to assess mortality. For short-term studies evaluating DEN-induced hepatic injury and compensatory proliferation, adult mice were treated with DEN by a single i.p. injection at a dose of 100 mg kg^{-1} of body weight and euthanized 2 h later. (ii) Streptozotocin was administered by i.p. injection (60 mg g^{-1}) to mice at postnatal day (P)1.5. All mice were fed a high-fat diet after weaning and histopathological studies were assessed at 27 weeks of age. (iii) Carbon tetrachloride was administered to adult mice via i.p. injection 3 times per week for 16 weeks. After the treatment, mice were euthanized for histopathological and biochemical studies and tumour analysis.

For PHx, adult mice were anaesthetized using a mixture of isoflurane and oxygen. Seventy percent of the liver was excised, which involves removal of the medial and left lateral lobes (used for histological and biochemical analyses). Liver proliferation, regeneration and histological and biochemical analysis were performed at 48 h and 15 days after PHx.

Immunohistochemical analyses. Liver and tumour tissues were fixed with phosphate-buffered 10% formalin and embedded in paraffin. Sections of 5 μm were stained with H&E for histopathological examination. Cell proliferation was assessed by immunohistochemical staining for Ki67 (ab15580, 1:100; Abcam), BrdU (ab6326, 1:100; Abcam) and phospho-Rb (S795) (9301, 1:100; Cell Signaling Technology).

BrdU treatment. Forty-eight hours after PHx, hepatocytes were labelled with BrdU in vivo by i.p. injection of 2 mg BrdU. After 2 h, mice were euthanized and livers extracted.

Assessment of HCC by magnetic resonance imaging. Tumours were monitored by MRI using administered gadoxetate disodium (Primovist; Bayer Healthcare) administered intravenously as a contrast medium to enhance focal hepatic tumours. Tumour volume was measured using OsiriX software (Pixmeo). Three-dimensional gradient echovolumetric imaging with minimum repetition time and echo time (3 ms and 1.5 ms, respectively), 20° flip angle and isotropic 150 μm spatial resolution, totalling 6 min acquisition time, were acquired around 10 min after Primovist injection (2 mg kg^{-1} body weight) via the tail vein. Images were acquired on an actively shielded 7 T horizontal scanner (Agilent) equipped with MM2 electronics, a 115/60 gradient insert coil, and a ^{1}H circular-polarization, transmit–receive volume coil of 35 mm inner diameter and 30 mm active length, built by Neos Biotec. Before contrast injection, each mouse was anaesthetized by inhalation of a mixture of isoflurane and oxygen (2–4%) and its breathing rhythm and temperature were monitored (Model 1024, SA Instruments). Animals were positioned supine on a customized bed with a built-in nose cone supplying inhalatory anaesthesia (1–2%) and kept at 35–37 °C by warm airflow throughout the experiment. After euthanasia, livers were collected, weighed, and the number of visible tumours was counted macroscopically and measured with a calliper. The figure shows axial slices extracted from the 3D volume dataset. Tumours were collected and frozen for biochemical analyses. For liver analysis, the largest lobe was fixed in formalin and embedded in paraffin. Sections were stained with H&E and examined microscopically.

Biochemical analysis. Total hepatic proteins were extracted from 30 mg frozen liver or tumour tissue using 500 μl of lysis buffer containing 50 mM Tris-HCl pH 7.5, 1 mM EGTA, 1 mM EDTA, 50 mM NaF, 1 mM sodium glycerophosphate, 5 mM pyrophosphate, 0.27 M sucrose, 1% Triton X-100, 0.1 mM PMSF, 0.1% β-mercaptoethanol, 1 mM sodium orthovanadate, 1 μg ml^{-1} leupeptin and 1 μg ml^{-1} aprotinin. Proteins were separated by sodium dodecyl sulfate–polyacrylamide gel electrophoresis (SDS–PAGE) and transferred onto 0.2 μm nitrocellulose membranes (BioRad). Membranes were blotted with primary antibodies targeting p38 (9212, 1:1,000; Cell Signaling Technology), p38γ (2307, 1:5,000; Cell Signaling Technology), a previously described p38γ antibody used for IP[19], phospho-p38 T180/Y182 (921, 1:1,000; Cell Signaling Technology), Rb (9313, 1:1,000; Cell Signaling Technology), phospho-Rb Ser 807/811 (8516, 1:1,000; Cell Signaling Technology), CDK2 ((78B2) 2546, 1:1,000 Cell Signaling Technology), PCNA (ab1897, 1:1,000; Abcam), vinculin (V4505, 1:1,000; Sigma-Aldrich), and GAPDH (G9245, 1:1,000; Sigma-Aldrich). Membranes were incubated with an appropriate horseradish peroxidase-conjugated secondary antibody (GE Healthcare) and developed using an enhanced chemiluminescent substrate (GE Healthcare). In western blots, each lane corresponds to a different mouse.

Hepatic, cardiac and renal injury was assessed from the levels of serum alanine aminotransferase, aspartate aminotransferase, creatine kinase, creatinine, alkaline phosphatase, and total bilirubin; all measurements were performed at the CNIC Animal Facility Unit.

Kinase assay. For the competitive kinase assays to evaluate the cooperation between CDK2 and p38γ, we used 0.5 μg of total protein and 0.5 μg of each kinase per reaction (Rb only, Rb + p38γ, Rb + CDK2/cyclin A, Rb + p38γ + CDK2/cyclin A). We added 100 μM ATP to each reaction at 30 °C for 15 min. To find all the residues phosphorylated by CDK2 and p38γ, we used 2 μg of total protein and 1 μg of each kinase per reaction (Rb only, Rb + p38γ, Rb + CDK2/cyclin A, Rb + p38γ + CDK2/cyclin A). We added 100 μM ATP to each reaction at 30 °C for 60 min.

Reactions were run on ExpressPlus PAGE acrylamide gels from GenScript, stained, and bands corresponding to Rb were then excised and analysed by mass spectrometry (MS) to identify phosphopeptides[8].

RNA isolation and quantitative PCR analysis. Total RNA was isolated from liver and tumour tissue with the RNeasy Mini Kit (Qiagen) with on-column DNase I digestion. RNA was quantified using a NanoDrop spectrophotometer. Complementary DNA synthesis was carried out using the High-Capacity cDNA Reverse Transcription Kit (Applied Biosystems). Expression of the housekeeping genes *Rn18s* and *Gapdh* was used for normalization. Quantitative PCR (qPCR) was performed using Fast SYBR Green (Applied Biosystems) on a 7900HT Fast Real-time PCR system (Applied Biosystems). Primer sequences were as follows (F, forward; R, reverse):

Gapdh F: TGAAGCAGGCATCTGAGGG, *Gapdh* R: CGAAGGTGGAAG AGTGGGA; *Rn18s* F: CAGCTCCAAGCGTTCCTGG, *Rn18s* R: GGCCTTCAAT TACAGTCGTCTTC; *Ccnd1* F: GGTCCATAGTGACGGTCAGGT, *Ccnd1* R: GCGTACCCTGACACCAATCTC; *Ccne1* F: GCCTTCACCATTCATGTGGAT, *Ccne1* R: TTGCTGCGGGTAAAGAGACAG; *Ccna1* F: GTGGCTCC

GACCTTTCAGTC, *Ccna1* R: CACAGTCTTGTCAATCTTGGCA; *Rb1* F: CCGTTTTCATGCAGAGACTAAA, *Rb1* R: GAGGTATTGGTGACAAGG TAGGA; *Cdk1* F: AGAAGGTACTTACGGTGTGGT, *Cdk1* R: GAGAGA TTTCCCGAATTGCAGT; *Cdk2* F: CCTGCTCATTAATGCAGAGGG, *Cdk2* R: GTGCTGGGTACACACTAGGTG; *Cdk4* F: ATGGCTGCCACTCGATATGAA, *Cdk4* R: TCCTCCATTAGGAACTCTCACAC; human *COL1A* F: GAGGGCCAAG ACGAAGACATC, human *COL1A* R: CAGATCACGTCA TCGCACAAC; human *ACTA2* F: AAAAGACAGCTACGTGGGTGA, human *ACTA2* R: GCCATGTT CTATCGGGTACTTC.

Cell lines and proliferation and transfection assays. We used HCC cell lines derived from human patients (HepG2, Huh7, Snu354, Snu398 and Snu449, NCBI BioSample) and wild-type human hepatocytes (HepaRG from Life Technologies). We first studied p38γ expression in cells derived from patients with HCC to avoid the unjustified use of mice. Cell lines were tested for mycoplasma contamination by PCR. Cells were cultured in DMEM (Sigma-Aldrich, D5796) supplemented with 10% FBS (HyClone, SV30160.03), L-glutamine (Lonza, 20 mM in 0.85% NaCl) and penicillin/streptomycin (Lonza, DE17-602E; 10,000 units of each antibiotic).

HepG2 and Snu398 cells were used for knock-down assays. shRNAs against p38γ were purchased from Dharmacon (V3LHS_636283 and V3LHS_636282).

To measure proliferation, HepG2 and Snu398 cells treated with shp38γ or shScramble were seeded in 24-well plates at 15×10^4 cells per well at different FBS concentrations (0.1%, 0.2%, 2% and 20%). Cells were counted after 48 h of incubation.

For colony-formation assays, 2×10^3 HepG2 and Snu398 treated with shp38γ or shScramble were seeded in a p100 Petri dish. After 2 weeks (without changing the medium) the colonies were fixed and stained with 0.1% crystal violet.

For soft agar assays, HepG2 shp38γ and HepG2 shScramble cells (10^5) were seeded in a p100 Petri dish between a base agar layer (0.5% agar, 1 × DMEM and 10% FBS) and a top agarose solution (0.7% agar, 1 × DMEM and 20% FBS). The medium was replenished every 3 days. After 20 days, plates were stained with 0.5% crystal violet, and colonies were counted using a light microscope.

HA-Rb wild-type and HA-RbΔCDK plasmids (Addgene; 58905 and 58906, respectively) were transfected into HEK 293T cells using the calcium phosphate transfection method. Cells were lysed 36 h post-transfection, and immunoprecipitation assays were performed.

Lentivirus and adeno-associated virus production. Lentiviruses were produced as described[4]. Transient calcium phosphate co-transfection of HEK-293T cells was carried out with shCDK1 (RMM4532-EG12534), shCDK2 (RMM4532-EG12534), shCDK4 (RMM4532-EG12567) or CDK6 (RMM4532-EG12571) from Dharmacon, together with pΔ8.9 and pVSV-G packaging plasmids. Supernatants containing the lentiviral particles were collected 48 h and 72 h after removal of the calcium phosphate precipitate, centrifuged at 700*g* at 4 °C for 10 min, and concentrated (×165) by ultracentrifugation for 2 h at 121,986*g* at 4 °C (Ultraclear Tubes, SW28 rotor and Optima L-100 XP Ultracentrifuge; Beckman). Viruses were resuspended in cold sterile PBS and titrated by qPCR.

AAV plasmids were cloned and propagated in the Stbl3 *Escherichia coli* strain (Life Technologies). pCEFL Flag p38γ D129A and pCEFL-p38α-D176AF327S[25] were cloned into a liver-specific HRC-hAAT promoter plasmid[26] to generate pAAV-HRC-hAAT-p38γact (AAVp38γ*). AAV2/8-CAG-Cre-WPRE was obtained from Harvard University. These AAV plasmids were packaged into AAV-9 or AAV-8 capsids to specifically target the liver, produced by the Viral Vector Unit at CNIC as described[8]. Adeno-associated viruses (serotypes AAV8 and AAV9) were produced in HEK-293T cells and collected from the supernatant. Mice were injected in the tail vein with 1×10^{11} adenoviral particles suspended in PBS.

Molecular dynamics simulations. Molecular dynamics simulations were used to study the spontaneous binding of the inhibitor RO3306 to the ATP-binding sites of p38γ, CDK1, CDK2 and p38α. The spontaneous binding of the inhibitor pirfenidone to the p38γ ATP-binding site was also studied. The parameters for RO3306 and pirfenidone in the molecular dynamics simulations were generated within the ANTECHAMBER module of AMBER 16 (ref. [27]) using the general AMBER force field (GAFF), with partial charges set to fit the electrostatic potential generated at the HF/6-31G(d) level by the RESP model. The charges were calculated according to the Merz-Singh-Kollman scheme using Gaussian 09.

Many crystal structures are available for the homologues p38α and p38β. However, p38γ has been crystallized only in the phosphorylated state and in the presence of an ATP derivative in the ATP-binding site (Protein Data Bank (PDB) accession number 1CM8). In this crystal structure, the loops corresponding to residues 34–39, 316–321 and 330–334 were not resolved. For the molecular dynamics simulations, we generated two models of p38γ using the SwissModel homology model server and 1CM8 (phosphorylated and ATP-bound state p38γ) and 3GP0 (inhibitor-bound state of p38β) as templates. Molecular dynamics simulations of CDK1 were carried out using PDB 5HQ0 as a reference, removing the crystallized ligand that occupies the ATP-binding site. Molecular dynamics simulations of CDK2 were performed using PDB 3PXR, corresponding to the apo CDK2 state. For p38α, PDB 3GI3 was used as a reference for starting the molecular dynamics simulations, removing the crystallized ligand occupying the ATP-binding site. In all cases, we placed RO3306 or pirfenidone in an arbitrary position in the solvent region (more than 20 Å away from the ATP-binding site). From these coordinates, we began unrestrained conventional molecular dynamics (cMD) simulations (250 ns) followed by accelerated molecular dynamics (aMD) simulations (1,500 ns for p38γ with RO3306, 2,000 ns for CDK1 with RO3306, 2,250 ns for CDK2 with RO3306, 2,000 ns for p38α with RO3306 and 2,000 ns for p38γ with pirfenidone) to allow the inhibitor to diffuse freely until it spontaneously associated with the protein surface, and finally targeted the ATP-binding site. Inhibitor binding was monitored throughout the simulations by plotting a selected distance between the hydrogen-bond acceptor of the inhibitor and the backbone of a residue located at the ATP-binding site responsible for the recognition and stabilization of the inhibitor (Met112 for p38γ and Met109 for p38α, and Leu83 for CDK1 and CDK2; see Extended Data Figs. 1, 10). Short distances indicate binding of RO3306 in the ATP-binding site. Spontaneous binding to p38γ was observed in five out of ten simulations (light purple, light and dark blue, light red, and teal in Extended Data Fig. 1b); in the case of CDK1, spontaneous binding was observed in two out of ten simulations (light blue and light pink). When binding occurs, RO3306 remains in the ATP-binding pocket for the rest of the simulation, thus indicating the strong affinity of the inhibitor towards p38γ and CDK1. By contrast, spontaneous binding does not occur in p38α or in only 1 out of 10 simulations in CDK2 (see Extended Data Fig. 1c). Comparison of the spontaneous binding events for p38γ and p38δ that were observed in 500 ns of aMD simulation time indicate that RO3306 has a higher affinity towards p38γ (RO3306 is bound to p38γ and p38δ for 19.7% and 5.5% of the simulation time, respectively; see Extended Data Fig. 1d).

Each system was immersed in a pre-equilibrated truncated octahedral box of water molecules with an internal offset distance of 10 Å, using the LEAP module. All systems were neutralized with explicit counterions (Na^+ or Cl^-). A two-stage geometry optimization approach was performed. First, a short minimization was made of the positions of the water molecules, with positional restraints on the solute by a harmonic potential with a force constant of 500 kcal mol^{-1} $Å^{-2}$. The second stage was an unrestrained minimization of all the atoms in the simulation cell. The systems were then gently heated through six 50-ps steps, each increasing the temperature by 50 K (0–300 K) under constant volume and using periodic boundary conditions and the particle mesh Ewald approach to introduce long-range electrostatic effects. For these steps, an 8 Å cutoff was applied to Lennard-Jones and electrostatic interactions. Bonds involving hydrogen were constrained with the SHAKE algorithm. Harmonic restraints of 10 kcal mol^{-1} were applied to the solute, and the Langevin equilibration scheme was used to control and equalize the temperature. The time step was kept at 2 fs during the heating stages, allowing potential inhomogeneities to self-adjust. Each system was then equilibrated for 2 ns with a 2-fs time step at a constant pressure of 1 atm. Finally, a 250 ns conventional molecular dynamics trajectory at constant volume and temperature (300 K) was collected, followed by ten replicas of 1,500 ns of dual-boost aMD[28,29] for p38γ in the presence of RO3306, ten replicas of 2,000 ns of aMD for CDK1 in the presence of RO3306, ten replicas of 2,250 ns of aMD for CDK2 in the presence of RO3306, ten replicas of 2,000 ns of aMD for p38α in the presence of RO3306, and five replicas of 2,000 ns of aMD for p38γ in the presence of pirfenidone. In total, we gathered 15 μs of aMD for p38γ, 20 μs of aMD for CDK1, 22.5 μs of aMD for CDK2, and 20 μs of aMD for p38α, all of them with RO3306, and 10 μs of aMD for p38γ with pirfenidone. These long-timescale unconstrained aMD simulations were performed with the aim of capturing several spontaneous binding events. aMD enhances the conformational sampling of biomolecules by adding a non-negative boost potential to the system when the system potential is lower than a reference energy:

$$V^*(\mathrm{r}) = V(\mathrm{r}), \;\; V(\mathrm{r}) \geq E,$$

$$V^*(\mathrm{r}) = V(\mathrm{r}) + \Delta V(\mathrm{r}) \; V(\mathrm{r}) < E,$$

where $V(\mathrm{r})$ is the original potential, E is the reference energy, and $V^*(\mathrm{r})$ is the modified potential. In the simplest form, the boost potential is given by

$$\Delta V(\mathrm{r}) = (E - V(\mathrm{r}))^2 / (\alpha + E - V(\mathrm{r})),$$

where α is the acceleration factor. As the acceleration factor α decreases, the energy surface becomes more flattened and biomolecular transitions between the low-energy states are increased.

Here, a total boost potential is applied to all atoms in the system in addition to a more aggressive dihedral boost, that is, (E_{dihed}, α_{dihed}; E_{total}, α_{total}), within the

dual-boost aMD approach. The acceleration parameters used in this study are as follows:

$$E_{\mathrm{dihed}} = V_{\mathrm{dihed-avg}} + 3.5 \times N_{\mathrm{res}},\ \alpha_{\mathrm{dihed}} = 3.5 \times N_{\mathrm{res}}/5;$$

$$E_{\mathrm{total}} = V_{\mathrm{total-avg}} + 0.2 \times N_{\mathrm{atoms}},\ \alpha_{\mathrm{total}} = 0.2 \times N_{\mathrm{atoms}},$$

where N_{res} is the number of protein residues, N_{atoms} is the total number of atoms, and $V_{\mathrm{dihed\_avg}}$ and $V_{\mathrm{total\_avg}}$ are the average dihedral and total potential energies calculated from 250 ns cMD simulations, respectively.

Statistical analysis and reproducibility. Data are expressed as mean ± s.e.m. Differences were analysed by Student's *t*-test, with significance assigned at $P < 0.05$. Fisher's exact test was used to compare HCC incidence. The Wilcoxon–Mann–Whitney rank-sum test was used to calculate the statistical significance of the observed differences between groups with different variances. The log-rank test was used to assess significance in the Kaplan–Meier analysis. GraphPad Prism version 5 software was used for calculations.

Sample-size estimates for animal experiments were determined using power calculations. GraphPad Prism version 5 software was used for statistical analyses. Unpaired Student's *t*-tests were used to determine the power ($a = 0.05$, two-tailed). We observed many statistically significant effects in the data, indicating that the effective sample size was sufficient for studying the phenomena of interest. The experiments using mice were randomized. Mice were grouped based on gender (male), genotype, treatments, weight and age, and were randomly selected. We were blinded to allocation during experiments and outcome assessment. For in vivo experiments, an investigator treated the mice and collected the tissue samples. These samples were assigned code numbers. The analyses—including qPCR, immunohistochemistry staining and western blotting—were performed by another independent investigator. Experiments were repeated two or three times. All attempts at replication were successful.

Figure 1. **a**–**d**, Representative of at least three independent experiments. **e**, Data are mean ± s.e.m. $n = 3$–5 fields from AlbCre mice: 0 h, $n = 3$; 48 h, $n = 5$; AlbCre-p38γ mice: 0 h, $n = 5$; 48 h, $n = 7$ mice. $^{***}P < 0.001$. Comparisons were made by one-way ANOVA coupled to Bonferroni's post-test. **f**, Data are mean ± s.e.m. $n = 2$–5 fields from AlbCre mice: 0 h, $n = 4$; 48 h, $n = 7$; AlbCre-p38γ mice: 0 h, $n = 4$; 48 h, $n = 6$ mice. $^{**}P < 0.01$; $^{***}P < 0.001$. Comparisons were made by one-way ANOVA coupled to Bonferroni's post-test. **h**, Representative of at least three independent experiments. 1 h, data are mean ± s.e.m. AlbCre mice: $n = 3$; AlbCre-p38γ mice: $n = 8$. $^{***}P < 0.001$. Comparisons were performed using the two-sided Student's *t*-test.

Figure 2. **a**, **b**, Representative of at least three independent experiments. **c**, Data are mean ± s.e.m. $n = 4$–5 fields from AlbCre mice: 0 h, $n = 7$; 48 h, $n = 7$; CDK1/2 KO mice: 0 h, $n = 3$; 48 h, $n = 3$; CDK1/2 KO AAVp38γ* mice: 0 h, $n = 4$; 48 h, $n = 4$ mice. $^{*}P < 0.05$. Comparisons were made by one-way ANOVA coupled to Kruskal–Wallis post-tests. **d**, Data are mean ± s.e.m. $n = 3$–5 fields from AlbCre mice: 0 h, $n = 7$; 48 h, $n = 7$; AlbCre-p38γ mice: 0 h, $n = 3$; 48 h, $n = 3$; AlbCre-p38γ AAVp38γ* mice: 0 h, $n = 3$; 48 h, $n = 3$. $^{*}P < 0.05$. Comparisons were performed by a one-way ANOVA coupled to Kruskal–Wallis post-tests.

Figure 3. **a**, Immunohistochemistry was performed in two independent experiments. **b**, Linear relationships from $n = 107$ individuals tested by Pearson's correlation; $P < 0.001$. **c**, Kaplan–Meier survival curves of patients stratified by low or high expression of p38γ, $n = 372$ individuals; Mantel–Cox log-rank test. $P = 0.0039$. **e**, **f**, Data are mean ± s.e.m. Mann–Whitney *U*-test (**e**) and two-sided Student's *t*-test (**f**) in AlbCre mice: $n = 11$, AlbCre-p38γ mice: $n = 5$. **g**, Kaplan–Meier analysis of survival in DEN-treated AlbCre mice: $n = 10$ and AlbCre-p38γ mice: $n = 11$ mice. Mantel–Cox log-rank test; $^{**}P < 0.01$.

Figure 4. **a**, Representative of at least three independent experiments. **b**, Data are mean ± s.e.m. AlbCre untreated mice: 0 h, $n = 10$; 48 h, $n = 5$; AlbCre-p38γ untreated mice: 0 h, $n = 10$; 48 h, $n = 7$; AlbCre mice: 0 h, $n = 10$; 48 h, $n = 10$; AlbCre-p38γ mice: 0 h, $n = 17$; 48 h, $n = 10$ pirfenidone-treated mice. One-way ANOVA; $^{***}P < 0.001$. **c**, Representative of at least three independent experiments. **d**, Data are mean ± s.e.m. Tumour number: control, $n = 20$; pirfenidone, $n = 13$; total tumour volume: control, $n = 18$; Pirfenidone, $n = 13$; maximum tumour: control, $n = 18$; pirfenidone, $n = 13$ mice. Mann–Whitney *U*-test; $^{*}P < 0.05$. **e**, Kaplan–Meier analysis of survival. Mantel–Cox log-rank test; $^{***}P < 0.001$. Control, $n = 6$; Pirfenidone-treated, $n = 9$ mice. **f**, Representative of at least three independent experiments. Each lane corresponds to a different liver or tumour sample.

Reporting summary. Further information on research design is available in the Nature Research Reporting Summary linked to this paper.

Data availability

The datasets supporting the findings of this study are available within the paper and its Supplementary Information. Source Data (gels and graphs) for Figs. 1–4 and Extended Data Figs. 1–10 are provided with the online version of the paper. There is no restriction on data availability.

20. González-Terán, B. et al. p38γ and p38δ reprogram liver metabolism by modulating neutrophil infiltration. *EMBO J.* **35**, 536–552 (2016).
21. Postic, C. & Magnuson, M. A. DNA excision in liver by an albumin-Cre transgene occurs progressively with age. *Genesis* **26**, 149–150 (2000).
22. Trakala, M. et al. Functional reprogramming of polyploidization in megakaryocytes. *Dev. Cell* **32**, 155–167 (2015).
23. Cubero, F. J. et al. Haematopoietic cell-derived Jnk1 is crucial for chronic inflammation and carcinogenesis in an experimental model of liver injury. *J. Hepatol.* **62**, 140–149 (2015).
24. Zheng, K., Cubero, F. J. & Nevzorova, Y. A. c-MYC—making liver sick: role of c-MYC in hepatic cell function, homeostasis and disease. *Genes (Basel)* **8**, 123 (2017).
25. Askari, N. et al. Hyperactive variants of p38α induce, whereas hyperactive variants of p38γ suppress, activating protein 1-mediated transcription. *J. Biol. Chem.* **282**, 91–99 (2007).
26. Miao, C. H. et al. Inclusion of the hepatic locus control region, an intron, and untranslated region increases and stabilizes hepatic factor IX gene expression *in vivo* but not *in vitro*. *Mol. Ther.* **1**, 522–532, (2000).
27. Case, D. A. et al. *AMBER v.16* (University of California, San Francisco, 2017).
28. Hamelberg, D., Mongan, J. & McCammon, J. A. Accelerated molecular dynamics: a promising and efficient simulation method for biomolecules. *J. Chem. Phys.* **120**, 11919–11929 (2004).
29. Hamelberg, D., de Oliveira, C. A. & McCammon, J. A. Sampling of slow diffusive conformational transitions with accelerated molecular dynamics. *J. Chem. Phys.* **127**, 155102 (2007).

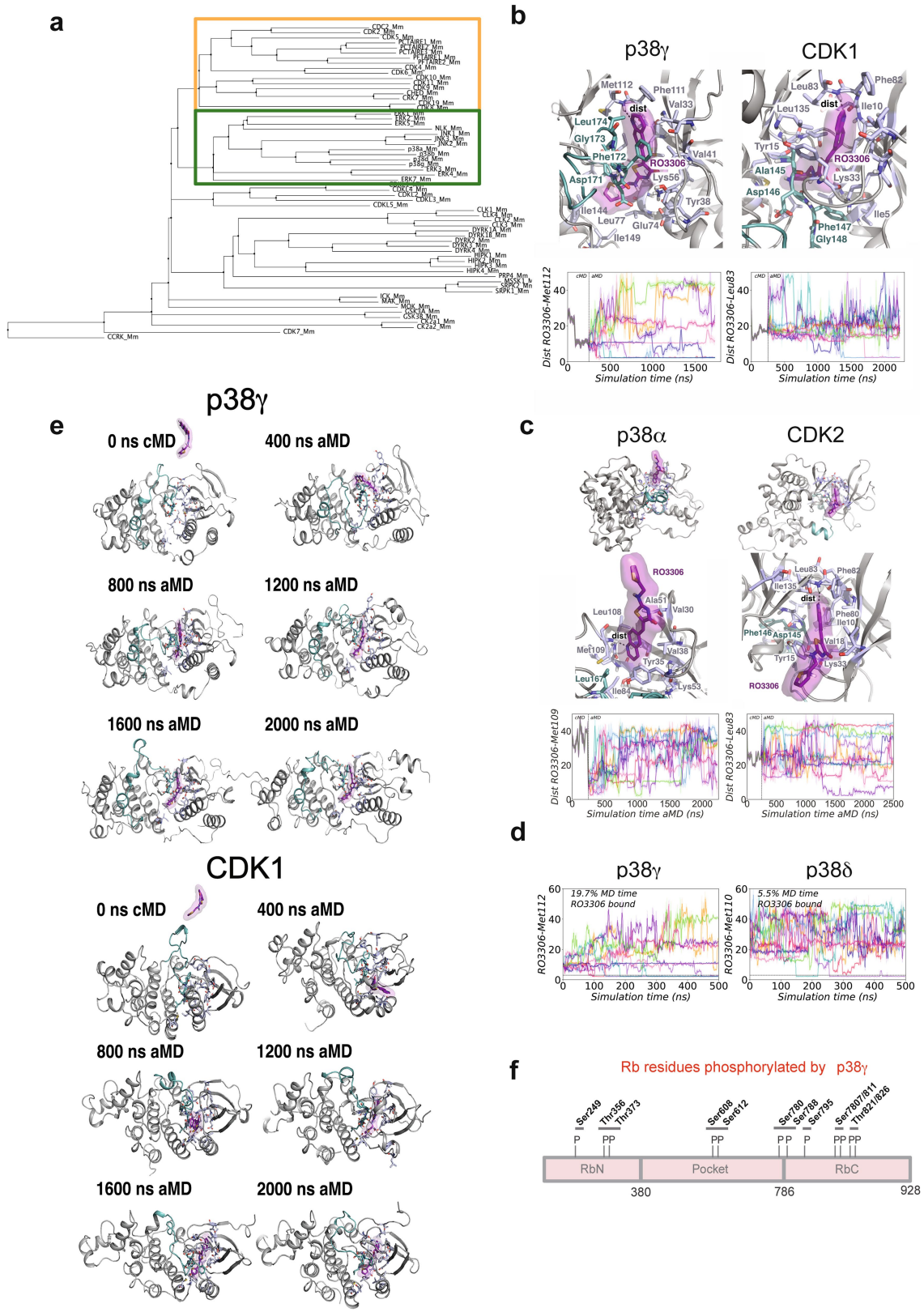

Extended Data Fig. 1 | Similarities between p38 MAPK proteins and CDKs. a, Phylogenetic tree of murine CMGC group kinases. The CDK family is boxed in orange, and the p38 family in green. **b**, **c**, Plot of the distance (in Å) between RO3306 and the ATP-binding site along the 10 aMD simulations of CDK1 and p38γ (**b**), and p38α and CDK2 (**c**), together with representative RO3306-bound conformations. Spontaneous binding of RO3306 occurs in 5/10 simulations with p38γ, 2/10 with CDK1, 0/10 with p38α, and 1/10 with CDK2. **d**, Comparison of spontaneous RO3306-binding events observed in 500 ns of aMD simulation time for p38γ and p38δ. **e**, Representative binding pathway obtained from aMD simulations of RO3306 with p38γ (top) and CDK1 (bottom). **f**, p38γ phosphorylation sites detected in Rb by an in vitro kinase assay followed by mass spectrometry.

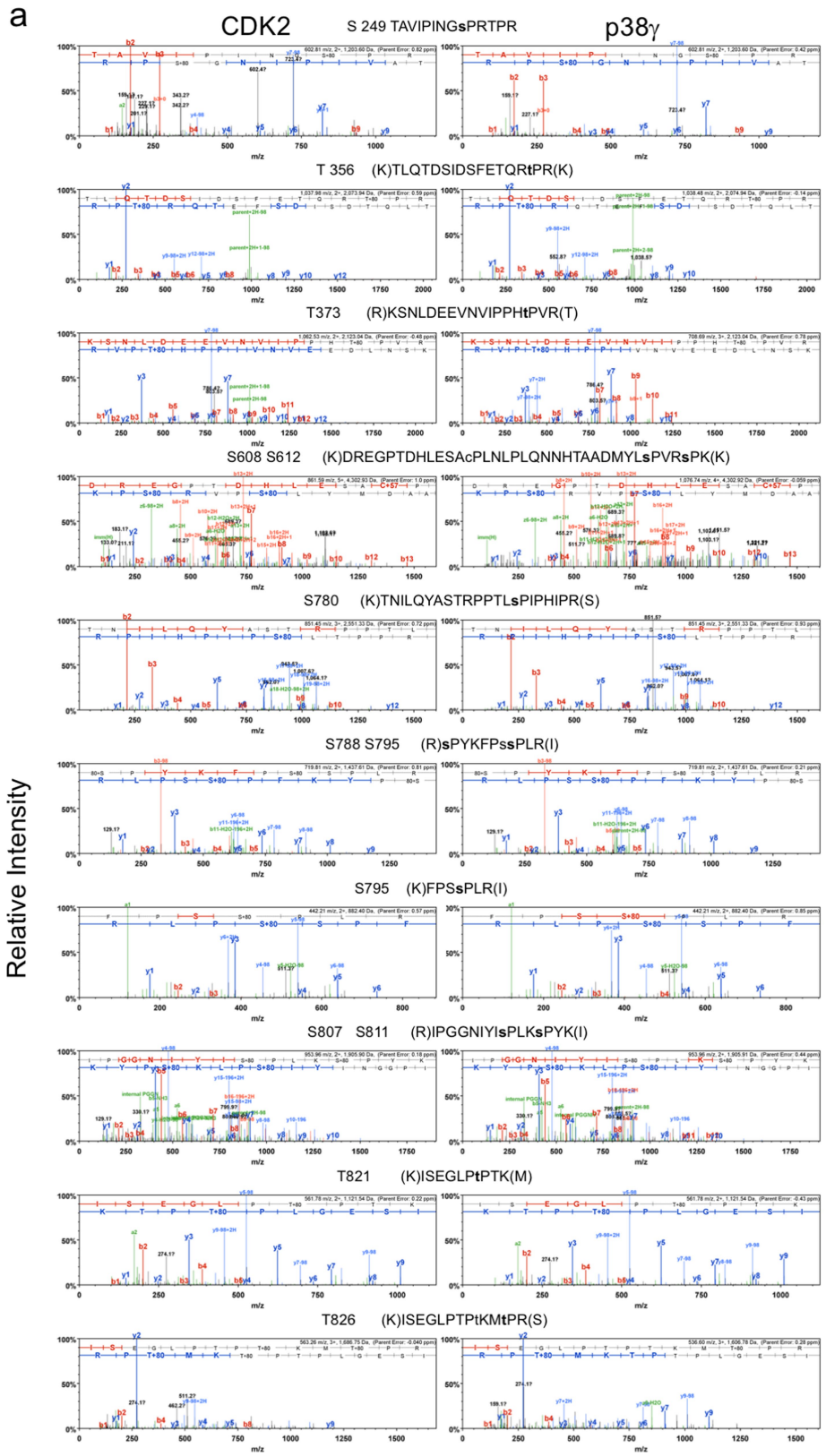

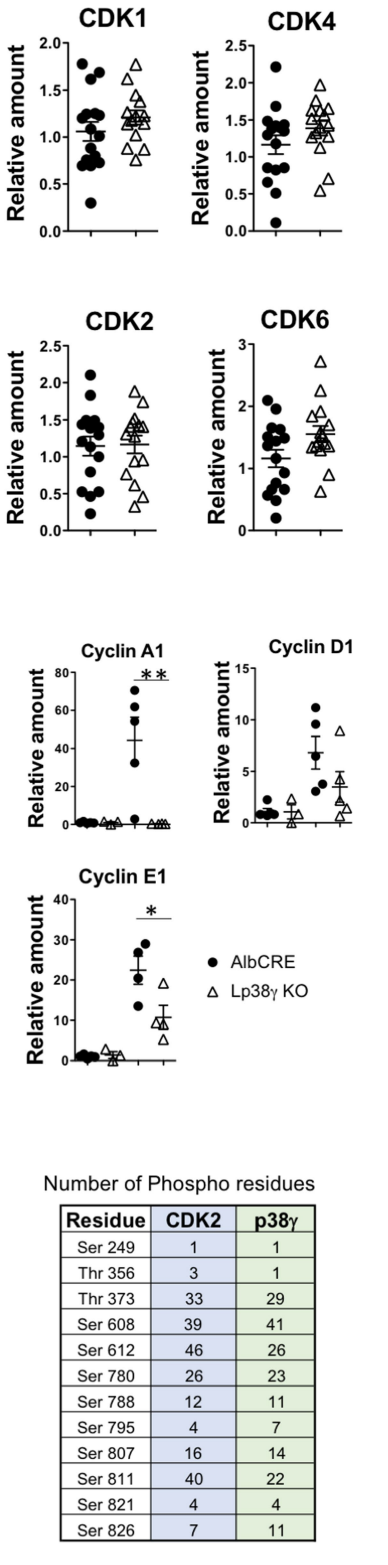

Number of Phospho residues

Residue	CDK2	p38γ
Ser 249	1	1
Thr 356	3	1
Thr 373	33	29
Ser 608	39	41
Ser 612	46	26
Ser 780	26	23
Ser 788	12	11
Ser 795	4	7
Ser 807	16	14
Ser 811	40	22
Ser 821	4	4
Ser 826	7	11

Extended Data Fig. 2 | Mass spectrometric analysis of in vitro phosphorylation of Rb by active p38γ or by CDK2–Cyclin A, and the expression of CDK and cyclin mRNA in AlbCre-p38γ mice. a, In an in vitro kinase assay, recombinant human Rb protein (2 μg) was incubated alone or in the presence of p38γ or CDK2–cyclin A kinases (1 μg) and 0.2 mM of cold ATP for 60 min. Interpreted MS/MS spectra demonstrating the phosphorylation of the indicated sites in Rb (in lower-case letters). The table shows the total spectral counts of the peptides where each phosphosite was identified. The data are representative of at least three independent experiments. No phosphopeptides were identified in the negative control without kinase. **b**, Quantitative PCR performed on liver extracts from AlbCre and AlbCre-p38γ mice. Expression was normalized to *Gapdh*. Data are shown as mean ± s.e.m. $n = 15$ mice for *Cdk1*, *Cdk2*, *Cdk4* and *Cdk6*, and $n = 6$ mice for cyclins A1 (*Ccna1*), D1 (*Ccnd1*) and E1 (*Ccne1*). $^{*}P < 0.05$; $^{**}P < 0.01$; $^{***}P < 0.001$. Comparisons were made by one-way ANOVA coupled to Bonferroni's post-tests.

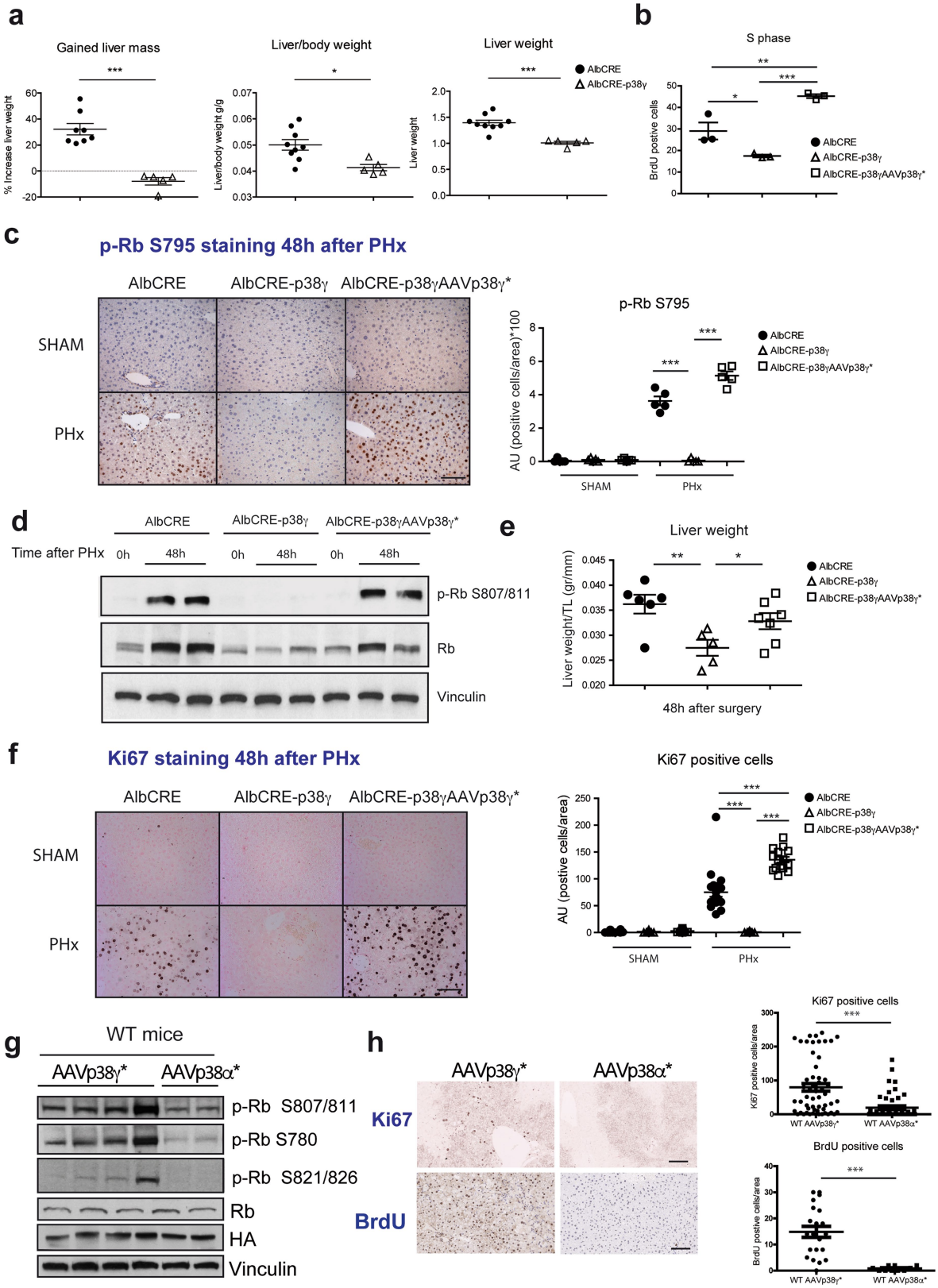

Extended Data Fig. 3 | See next page for caption.

Extended Data Fig. 3 | Expression of active p38γ in hepatocytes reverts liver proliferation in AlbCre-p38γ mice. AlbCre control mice, AlbCre-p38γ mice and AlbCre-p38γ mice infected with AAV expressing active p38γ (AlbCre-p38γ AAVp38γ*) were subjected to 70% PHx or a sham procedure. **a**, Gained liver mass, liver weight and liver:body mass ratio were measured 15 days after PHx and expressed as mean ± s.e.m. Gained liver mass: AlbCre mice, $n = 8$; and AlbCre-p38γ mice, $n = 5$; Liver:body weight: AlbCre mice, $n = 9$; AlbCre-p38γ mice, $n = 5$; Liver weight: AlbCre mice, $n = 9$; AlbCre-p38γ mice, $n = 5$. Comparisons were performed using a two-sided Student's *t*-test; $*P < 0.05$; $**P < 0.01$. **b**, BrdU incorporation quantified by cytometry. Data are mean ± s.e.m. $n = 3$. Comparisons were performed using a one-way ANOVA coupled to Bonferroni's post-tests; $***P < 0.001$; $*P < 0.05$; $**P < 0.01$. **c**, pRb Ser795 immunostaining in livers 48 h after PHx. Left, representative images. Scale bar, 100 μm. Right, quantification. Data are mean ± s.e.m. $n = 5$ mice. Comparisons were made by one-way ANOVA coupled to Bonferroni's post-tests; $***P < 0.001$. **d**, Immunoblot analysis of liver extracts with antibodies against phospho-Rb S807/S811, Rb, p38γ and vinculin (as a loading control). Each lane corresponds to a different mouse. The data are representative of at least three independent experiments. **e**, Liver:tibia length ratio, expressed as mean ± s.e.m. $n = 6$ mice. Comparisons were made by one-way ANOVA coupled to Bonferroni's post-tests; $*P < 0.05$; $**P < 0.01$. **f**, Hepatocyte proliferation analysed by Ki67 immunostaining 48 h after PHx. Left, representative images. Scale bar, 100 μm. Right, quantification of Ki67-positive cells, shown as mean ± s.e.m. Comparisons were performed using a one-way ANOVA coupled to a Kruskal–Wallis post-test. **g**, Wild-type mice infected with AAV expressing active p38γ (AAVp38γ*) or active p38α (AAVp38α*) were subjected to 70% PHx. Rb phosphorylation at the specified residues was assessed by western blot 48 h after PHx. Anti haemagglutinin (HA)-tag antibody was used as control of liver infection by AAVp38γ* and AAVp38α*; each lane corresponds to a different mouse. The data are representative of at least three independent experiments. **h**, Left, hepatocyte proliferation 48 h after PHx was studied by Ki67 immunostaining (top) or BrdU incorporation (bottom) in immunohistological liver sections. Scale bar, 100 μm. Right, quantification of Ki67- and BrdU-positive cells, shown as mean ± s.e.m. $n = 5$ counted areas from AlbCre mice: 0 h, $n = 4$; 48 h, $n = 4$; AlbCre-p38γ mice: 0 h, $n = 3$; 48 h, $n = 3$; AlbCre-p38γ AAVp38γ* mice: 0 h, $n = 3$; 48 h, $n = 3$; $n = 5$–25 counted areas from wild-type AAVp38γ* mice: $n = 4$; and wild-type AAVp38α* mice: $n = 2$. Comparisons were performed using a two-sided Student's *t*-test; $***P < 0.001$; $*P < 0.05$; $**P < 0.01$.

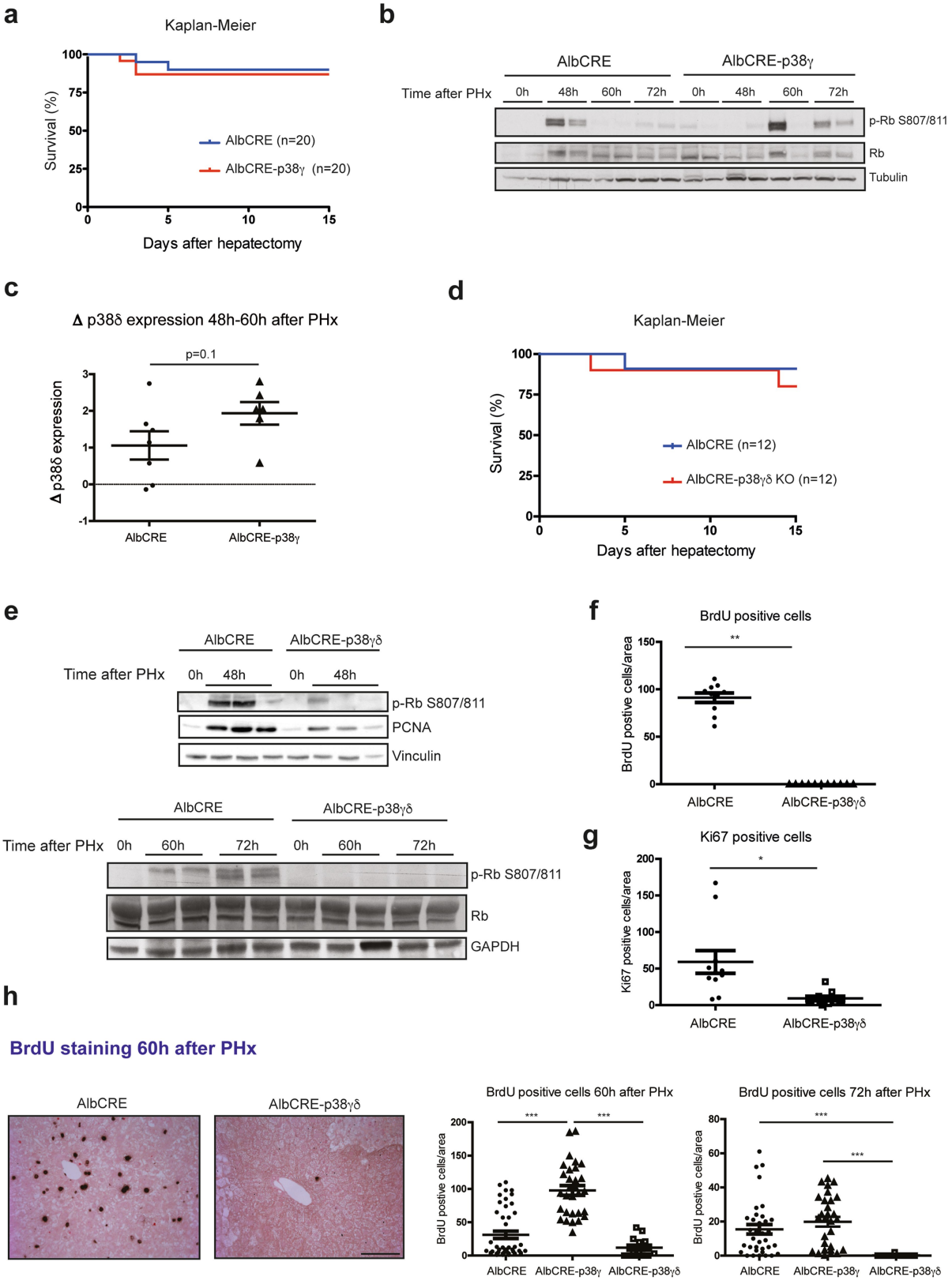

Extended Data Fig. 4 | See next page for caption.

Extended Data Fig. 4 | p38δ partially compensates for the lack of p38γ. **a**, Kaplan–Meier analysis of survival in PHx-treated AlbCre and AlbCre-p38γ mice. $n = 20$ mice per genotype. Mantel–Cox log-rank tests were used. **b**, Rb phosphorylation in the liver was studied in AlbCre and AlbCre-p38γ mice by western blotting with the indicated antibody 48 h, 60 h and 72 h after PHx; each lane corresponds to a different mouse. The data are representative of at least three independent experiments. **c**, p38δ expression was studied by qPCR at different time points after PHx and its change in expression was represented. AlbCre mice: $n = 7$ and AlbCre-p38γ mice: $n = 6$. Comparisons were performed using a two-sided Student's *t*-test. **d**–**h**, AlbCre control mice and AlbCre-p38γδ mice were subjected to 70% PHx or a sham procedure and were analysed after 48 h, 60 h or 72 h. **d**, Kaplan–Meier analysis of survival. A Mantel–Cox log-rank test was used. **e**, Immunoblot analysis of liver extracts from AlbCre-p38γδ mice with antibodies against phospho-Rb S807/S811, Rb, p38γ and vinculin (loading control); each lane corresponds to a different mouse. The data are representative of at least three independent experiments. **f**, **g**, Hepatocyte proliferation was analysed by BrdU incorporation (**f**; two-sided Student's *t*-test; $^{**}P < 0.05$) and Ki67 immunostaining (**g**; two-sided Student's *t*-test with Welch's correction; $^{*}P < 0.01$) 48 h after PHx in AlbCre-p38γ ($n = 3$) and AlbCre-p38γδ ($n = 3$) mice. **h**, Hepatocyte proliferation was analysed by BrdU incorporation 60 h and 72 h after PHx in AlbCre mice (60 h, $n = 9$; 72 h, $n = 7$), AlbCre-p38γ mice (60 h and 72 h, $n = 6$) and AlbCre-p38γδ mice (60 h and 72 h, $n = 3$). Comparisons were performed using a one-way ANOVA coupled to Bonferroni's post-tests; $^{***}P < 0.001$. Left, representative images. Scale bar, 50 μm. Right, quantification of Ki67- and BrdU-positive cells. Data are mean ± s.e.m. $n = 5$ counted areas from the specified number of mice.

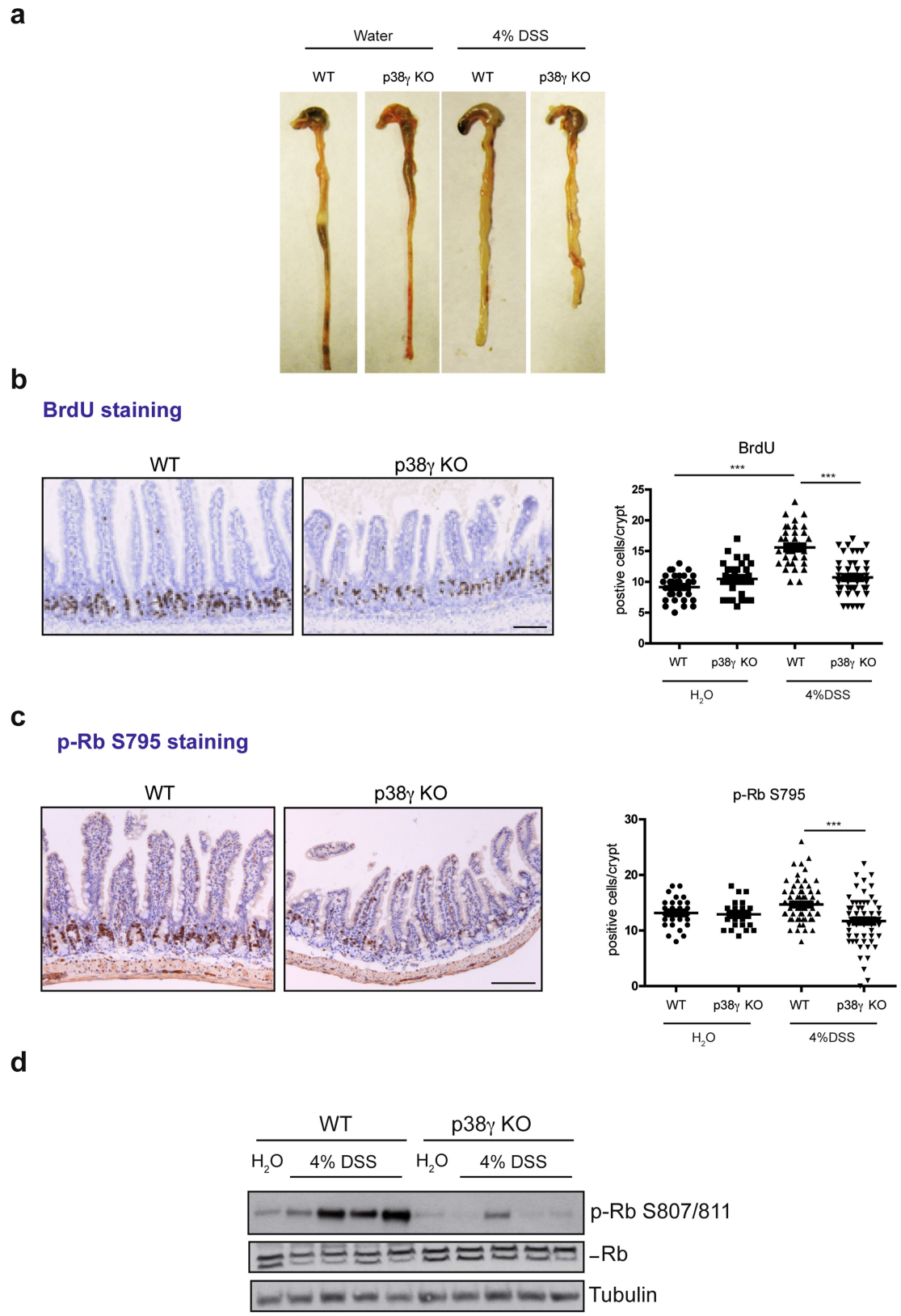

Extended Data Fig. 5 | Reduced epithelial proliferation and Rb phosphorylation in the absence of p38γ after treatment with dextran sodium sulfate. Wild-type and p38γ knockout mice were treated for 6 days with dextran sodium sulfate (DSS) administered in drinking water. **a**, Representative images showing the shortening of the colon after DSS treatment. **b**, Immunohistochemical staining (left) and BrdU quantification (right) in colon tissue sections of DSS-treated wild-type and p38γ knockout mice. **c**, Immunohistochemical staining (left) and phospho-Rb S795 quantification (right). Quantification is shown as mean ± s.e.m. $n = 5$–10 fields from wild-type control (H_2O) mice: $n = 5$; wild-type DSS-treated mice: $n = 7$; p38γ KO control mice: $n = 5$; p38γ KO DSS-treated mice: $n = 9$. In **b**, **c**, comparisons were made using a one-way ANOVA coupled with Bonferroni's multiple comparison test; $^{**}P < 0.01$; $^{***}P < 0.001$. Scale bar, 100 μm. d, Immunoblot analysis of Rb phosphorylation in the intestine, detected with the indicated antibody; each lane corresponds to a different mouse. The data are representative of at least three independent experiments.

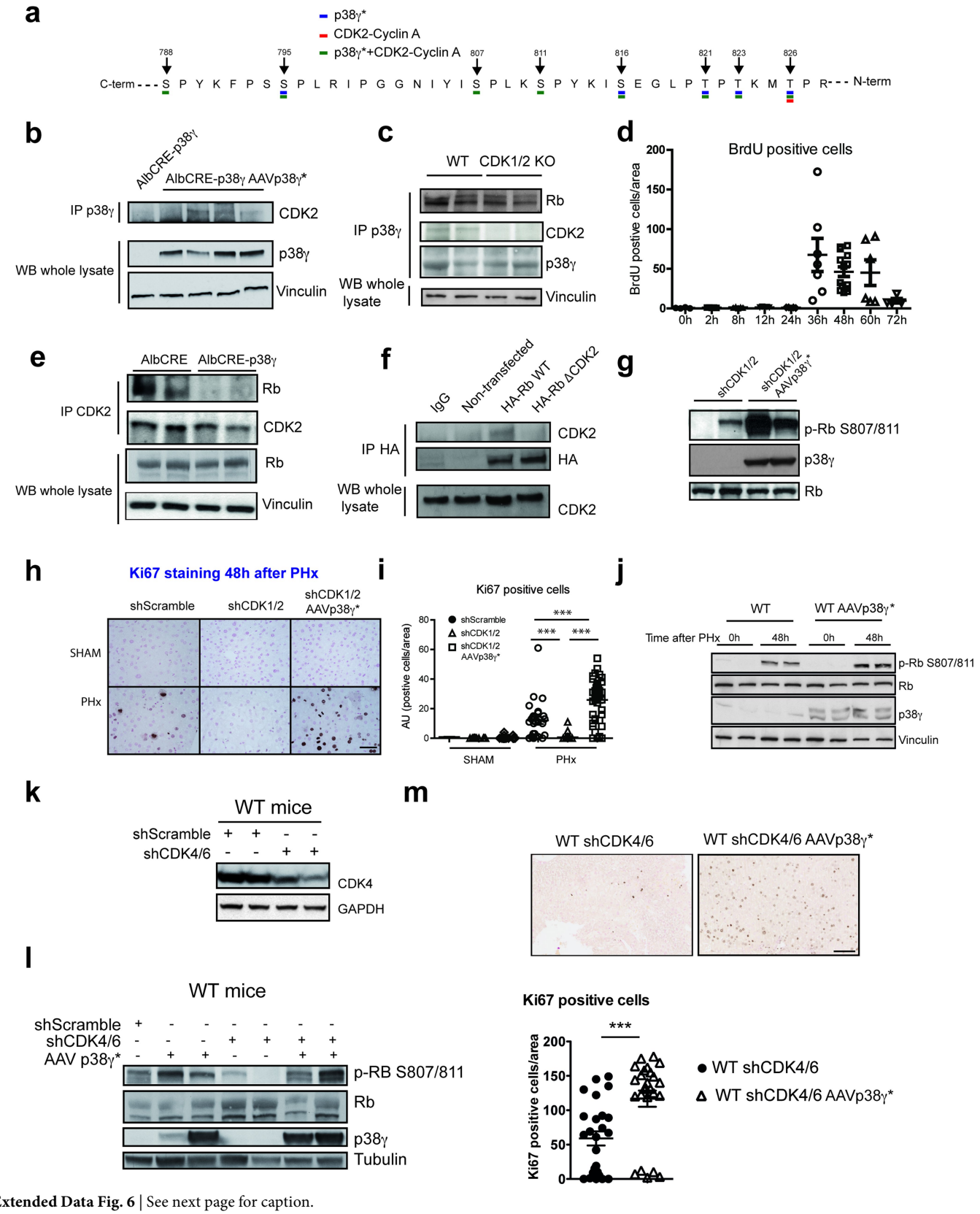

Extended Data Fig. 6 | See next page for caption.

Extended Data Fig. 6 | p38γ and CDKs cooperate in the induction of Rb phosphorylation and liver proliferation. a, In vitro kinase assay, in which phosphorylation sites identified by mass spectrometry are underlined. **b**, Immunoblot analysis of CDK2 in p38γ immunoprecipitates from the liver of AlbCre-p38γ mice with or without infection with AAV expressing active p38γ (AAVp38γ*). **c**, Immunoblot analysis of Rb expression in the liver in wild-type and CDK1/2 KO mice (AAV2/8-Cre-infected) in steady state. **d**, BrdU immunostaining analysis after PHx. Quantification is shown as mean ± s.e.m. $n = 5$ fields: 0 h, $n = 4$; 2 h, $n = 5$; 8 h, $n = 5$; 12 h, $n = 5$; 24 h, $n = 5$; 36 h, $n = 7$; 48 h, $n = 14$; 60 h, $n = 6$; 72 h, $n = 4$ mice. Comparison was performed using a one-way ANOVA coupled with Bonferroni's multiple comparison test. **e**, Immunoblot analysis in livers from AlbCre and AlbCre-p38γ mice. **f**, Immunoprecipitation–immunoblot analysis of the interaction of CDK2 with wild-type and nonphosphorylatable Rb in HEK-293T cells transfected with human HA-Rb wild-type or HA-Rb ΔCDK (nonphosphorylatable by CDKs). **g–m**, Wild-type mice were injected with lentivirus containing shScramble control or short hairpin RNA (shRNA) targeting CDK1/2 (shCDK1/2) or CDK4/6 (shCDK4/6) with or without AAV expressing active p38γ (AAVp38γ*). Mice were subjected to PHx or to a sham procedure. **g**, **k**, **l**, Immunoblot analysis. Hepatocyte proliferation was analysed by Ki67 immunostaining 48 h after PHx. Scale bars, 50 μm. **h**, **i**, **m**, Hepatocyte proliferation was analysed 48 h after PHx. **h**, Ki67 immunostaining. Scale bar, 100 μm. **i**, Ki67-positive cell quantification is shown as mean ± s.e.m. $n = 5$–10 counted areas from wild-type mice: 0 h, $n = 2$; 48 h, $n = 3$; shCDK1/2 mice: 0 h, $n = 3$; 48 h, $n = 4$; shCDK1/2 mice: 0 h, $n = 4$; 48 h, $n = 4$; AAVp38γ* mice: 0 h, $n = 4$; 48 h, $n = 5$. One-way ANOVA coupled with Bonferroni's multiple comparison test; $^{***}P < 0.001$. **m**, $n = 5$ counted areas from $n = 5$ mice). Scale bar, 100 μm. Comparisons were made by two-sided Student's *t*-test; $^{***}P < 0.001$. In the western blots, each lane corresponds to a different mouse and is representative of at least three independent experiments.

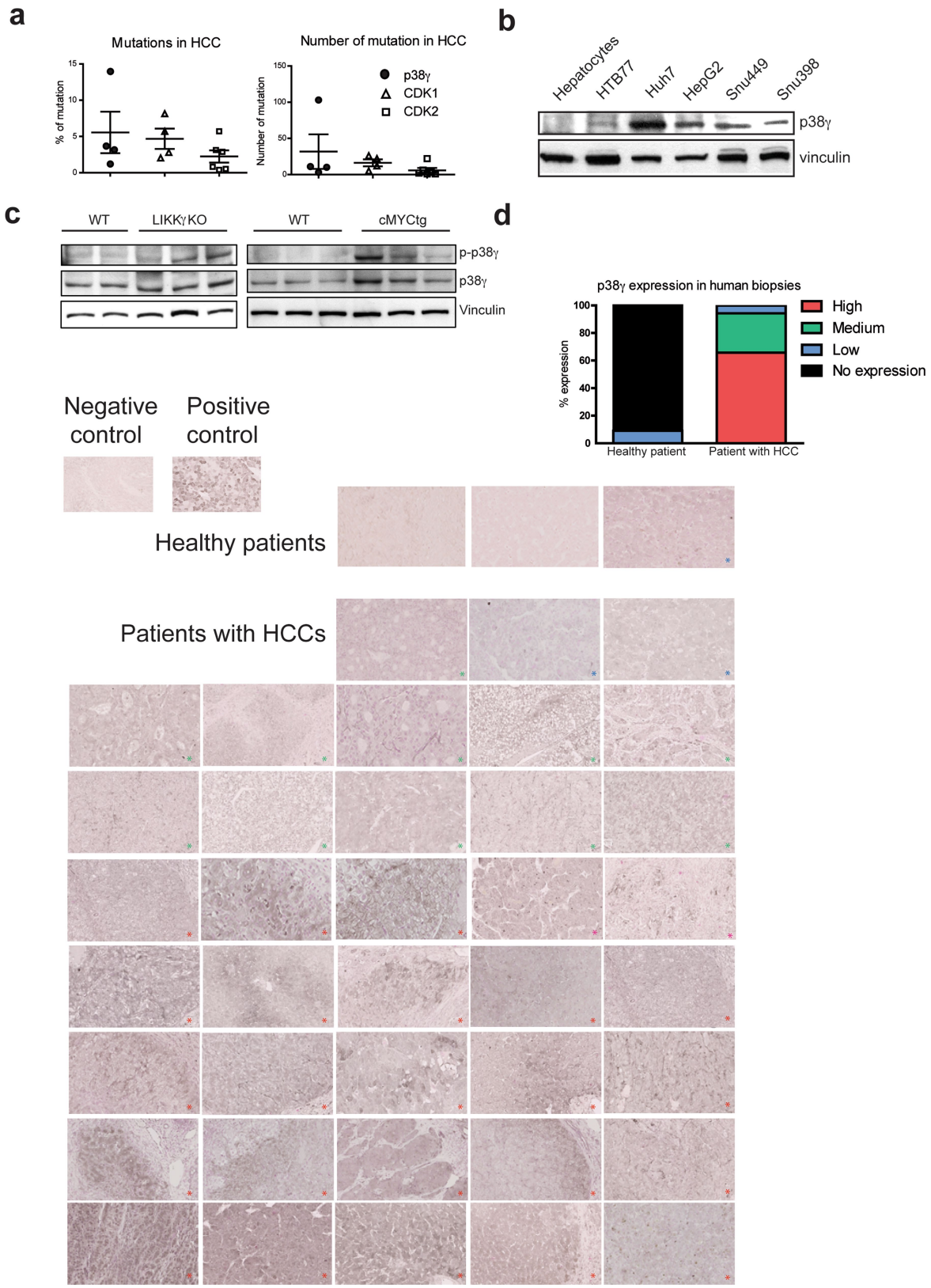

Extended Data Fig. 7 | See next page for caption.

Extended Data Fig. 7 | p38γ expression is increased in human HCC. **a**, Percentage of patients with HCC with mutations in p38γ, CDK1 and CDK2 and the number of HCC mutations in p38γ, CDK1 and CDK2. Data were obtained from the International Cancer Genome Consortium (data from 17 July 2017). **b**, Expression of p38γ in human primary hepatocytes and in human HCC cell lines (Huh7, HepG2, Snu449 and Snu398) and another type of cancer cells (HTB77). **c**, Immunoblot analysis of phospho-p38γ and total p38γ in liver extracts from mice lacking IKKγ in the liver (LIKKγKO) and control littermates (WT; left) and from c-Myc transgenic mice (cMYCtg) and wild-type counterparts (right). p38γ phosphorylation was detected only in mice lacking IKKγ specifically in the liver or overexpressing c-Myc. Vinculin served as a loading control. In the western blots each lane corresponds to a different mouse and is representative of at least three independent experiments. **d**, Immunohistochemical staining of p38γ in human liver with HCC. Negative control, p38γ knockout mice; positive control, p38γ knockout mice infected with human AAVp38γ. The chart shows stratification of p38γ expression in human liver samples as no expression, low, medium, and high expression ($n = 46$ patients with HCC and $n = 11$ healthy patients).

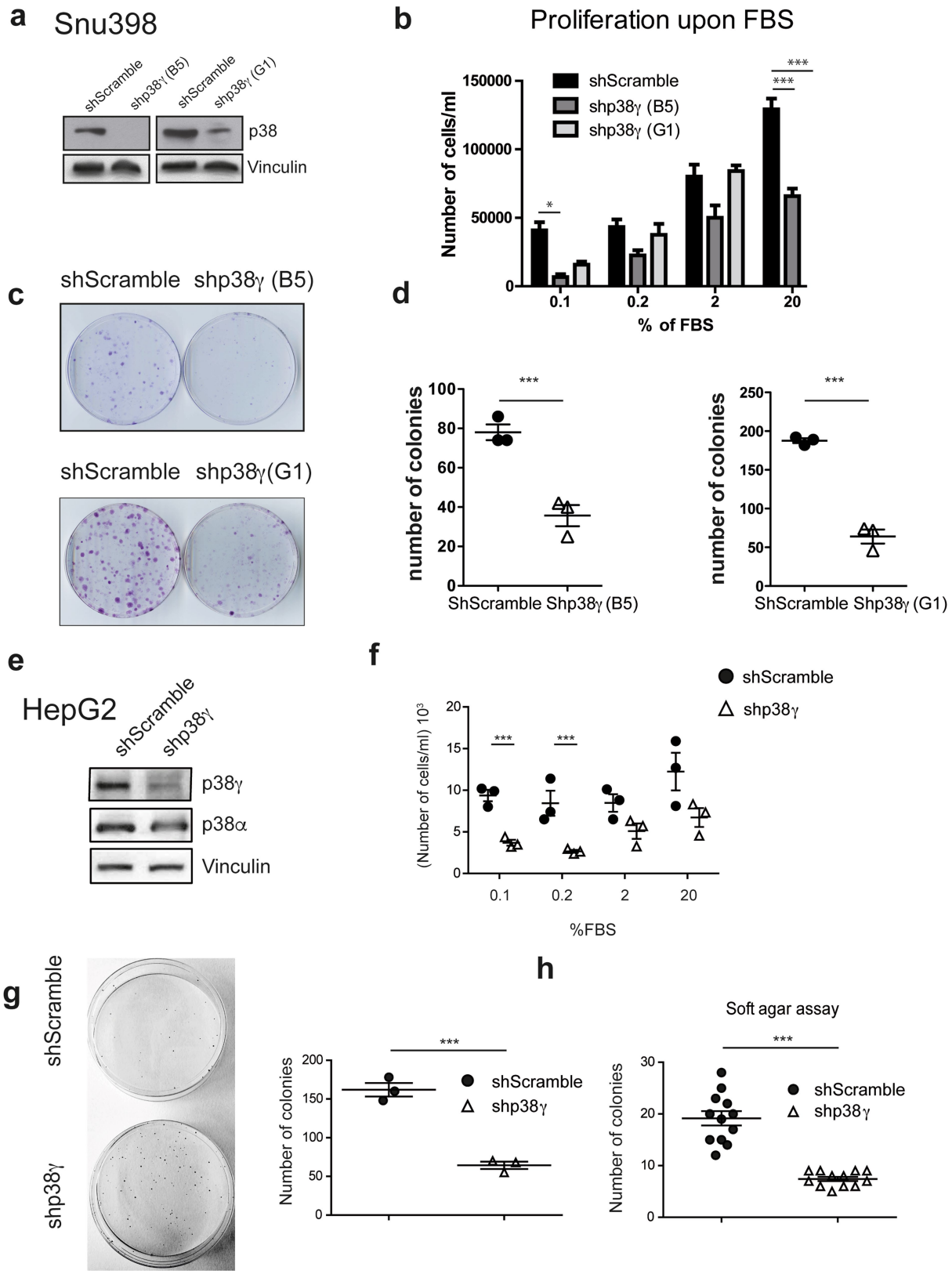

Extended Data Fig. 8 | See next page for caption.

Extended Data Fig. 8 | p38γ expression is necessary for Snu398 and HepG2 proliferation. a, Immunoblot analysis of Snu398 cells treated with lentiviral particles containing two p38γ-targeting shRNAs (B5 or G1) or shScramble. Representative western blot of at least three independent experiments. **b**, Growth of Snu398 cells infected with shp38γ or shScramble. Cells were plated and cultured for 2 days in medium supplemented with different serum concentrations. Relative cell numbers were measured by crystal violet staining. Data are mean ± s.e.m. ($n = 12$). Comparisons were made by two-way ANOVA; $^{***}P < 0.001$. **c**, Colony-formation assay of Snu398 cells infected with shp38γ or shScramble. Representative images are shown. **d**, Cells were grown in DMEM with 10% serum. The number of colonies with >10 cells was counted after 15 days. Data are mean ± s.e.m. ($n = 3$) and are represe*n*tative of results from three independent experiments. Comparisons were made by two-sided Student's *t*-test; $^{**}P < 0.01$; $^{***}P < 0.001$. **e**, Immunoblot analysis in HepG2 cells treated with lentiviral particles containing an shRNA against p38γ or Scramble control. Representative western blot of at least three independent experiments. **f**, Growth of HepG2 cells infected with shp38γ or shScramble. Cells were plated and cultured for 2 days in medium supplemented with different serum concentrations. Relative cell numbers were measured by crystal violet staining. Data are mean ± s.e.m. ($n = 3$) and are representative of results from three independent experiments. Comparisons were made by two-way ANOVA; $^{***}P < 0.001$. **g**, Left, colony-formation assay of HepG2 cells infected with shp38γ or shScramble. Representative images are shown. Cells were grown in DMEM with 10% serum. Right, the number of colonies with >10 cells was counted after 15 days. Data are mean ± s.e.m. ($n = 3$). Comparisons were made by two-sided Student's *t*-test; $^{***}P < 0.001$. **h**, Soft agar assay of HepG2 cells infected wi*t*h shp38γ or shScramble. Cells were grown in DMEM with 10% serum. The number of colonies with >10 cells was counted after 20 days. Data are mean ± s.e.m. ($n = 12$). Comparisons were made by Mann–Whitney *U*-test; $^{***}P < 0.001$.

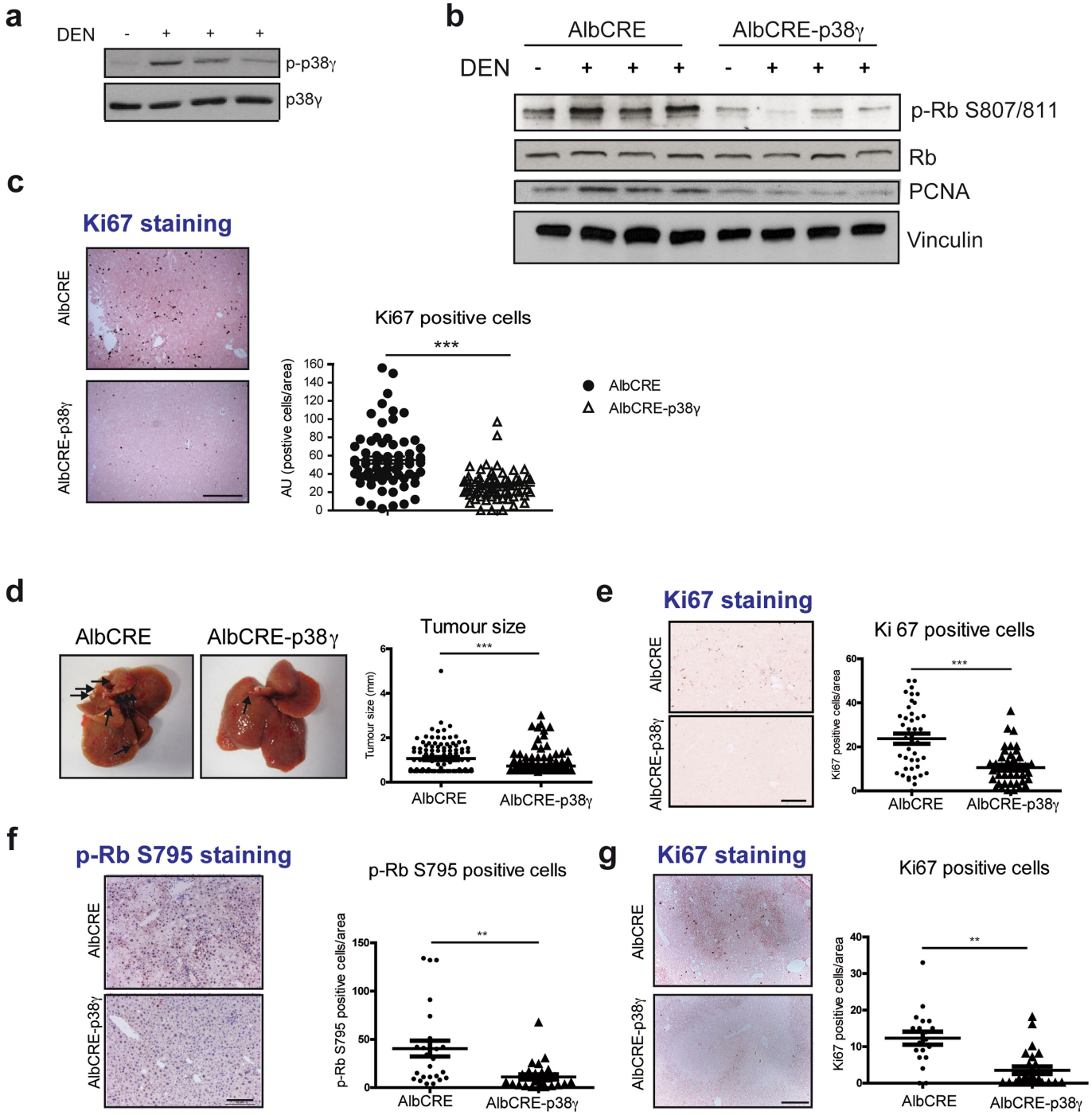

Extended Data Fig. 9 | AlbCre-p38γ mice are protected against carbon tetrachloride-induced liver damage and HCC induced by type 1 diabetes. a, Immunoprecipitation–immunoblot analysis of phosphorylated and total p38γ in liver extracts from AlbCre control mice, showing p38γ activation upon acute treatment with DEN (100 mg kg^{-1} for 2 h). Liver lysates (2 mg) were immunoprecipitated with anti-p38γ antibody followed by immunoblotting as indicated. **b**, Immunoblot analysis of Rb S807/S811 phosphorylation and proliferating cell nuclear antigen content in livers of AlbCre mice and AlbCre-p38γ mice 1 month after injection of DEN. Vinculin is shown as a loading control. **c**, Representative images of Ki67 immunohistochemistry in livers of AlbCre and AlbCre-p38γ mice 8 months after injection of DEN. Scale bar, 500 μm. Data are mean ± s.e.m. $n = 10$ fields in $n = 7$ mice. Two-sided Student's *t*-test; $^{***}P < 0.001$. **d**, **e**, AlbCre and AlbCre-p38γ mice were injected with 2 ml kg^{-1} of carbon tetrachloride (v/v) in 20% corn oil, three times per week for 14 weeks. All mice were fed a high-fat diet. **d**, Representative images of liver tumours (left) and quantification of tumour size (right). Comparisons were made by a two-tailed Student's *t*-test with Welch's correction; $^{***}P < 0.001$. **e**, Immunohistochemical staining and Ki67 quantification of liver tissue sections. Comparisons were performed with a two-sided Student's *t*-test; $^{***}P < 0.001$. Scale bar, 100 μm. Quantification is shown as mean ± s.e.m. $n = 5$ fields from $n = 9$ mice. f, g, Streptozotocin was subcutaneously injected (60 mg g^{-1}) into AlbCre and AlbCre-p38γ mice at P1.5. All mice were fed a high-fat diet and histopathologically assessed at 27 weeks of age. **f**, Immunohistochemical staining for phosphor-Rb S795 of liver tissue sections. AlbCre mice: $n = 5$; AlbCre-p38γ mice: $n = 5$. Comparisons were performed using a two-tailed Student's *t*-test with Welch's correction; $^{***}P < 0.001$. Scale bar, 100 μm. g, Ki67 staining on liver tissue sections. AlbCre mice, $n = 4$; AlbCre-p38γ mice, $n = 5$. Quantification is shown as mean ± s.e.m. $n = 2$–6. Scale bar, 100 μm. Comparisons were performed using a two-sided Student's *t*-test;$^{**}P < 0.01$.

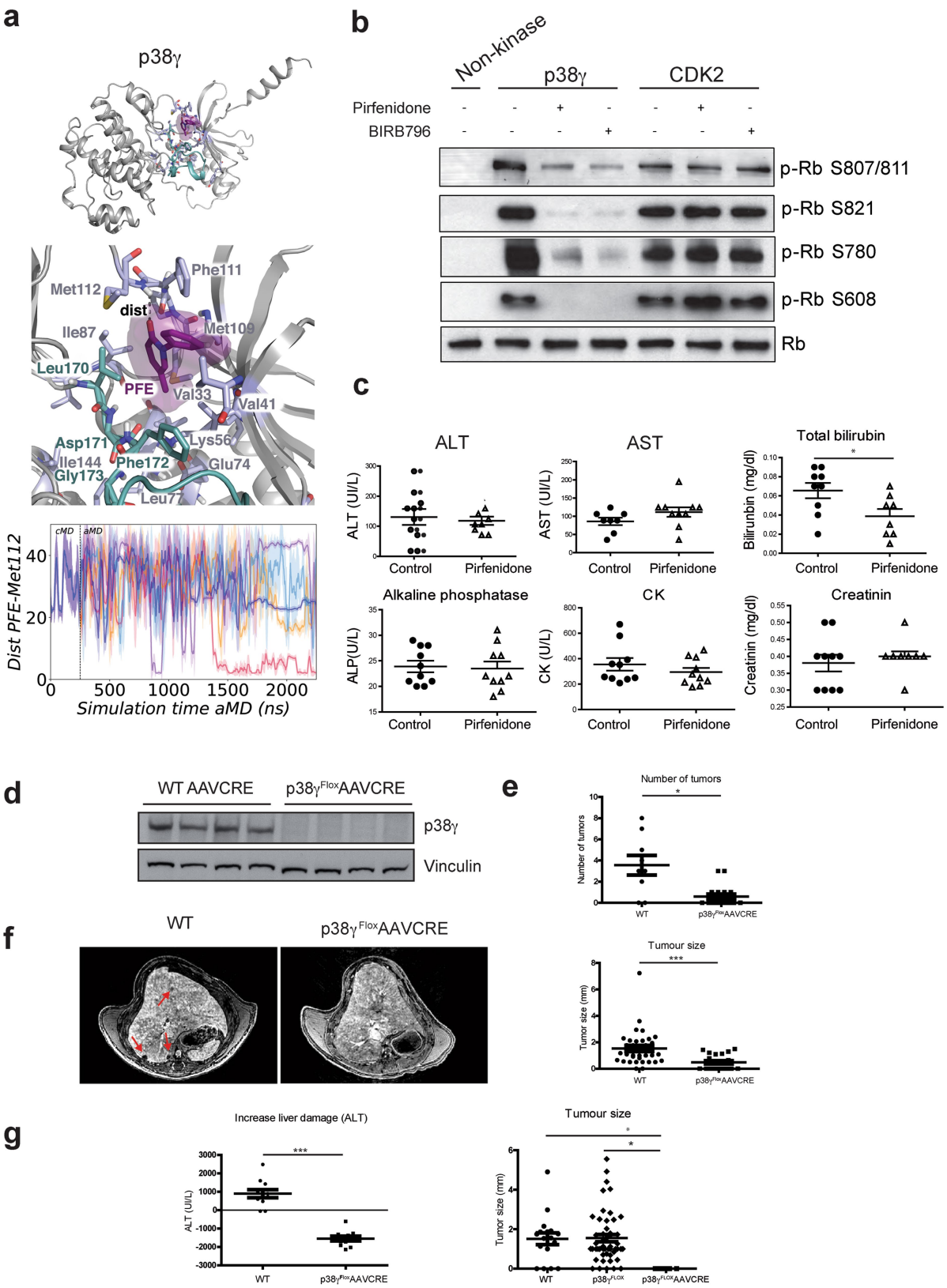

Extended Data Fig. 10 | See next page for caption.

Extended Data Fig. 10 | p38γ deletion or inhibition protects against DEN-induced HCC. a, Top, representative conformations of p38γ and the ATP-binding site of p38γ, both with the inhibitor pirfenidone bound (in purple), extracted from the molecular dynamics simulations. Middle, the activation loop of p38γ is shown in teal and other relevant ATP-binding site residues are shown in light blue. Bottom, plot of distance (in Å) between the oxygen of the pirfenidone carbonyl group and the amide backbone of p38γ Met112 during the molecular dynamics simulations for the five replicas (shown in different colours). Short distances indicate binding of pirfenidone in the ATP-binding site. Spontaneous binding of pirfenidone to p38γ was observed in one out of five simulations. **b**, Western blot of phosphorylated Rb. 10 μM BIRB796 or pirfenidone were added 30 min before the kinase assay. Representative western blot of at least three independent experiments. **c**, Wild-type mice were untreated (control) or treated with pirfenidone for 10 weeks and blood concentrations of the following selected parameters were assayed: alanine aminotransferase (ALT), as a readout of hepatic injury (comparisons were made by two-sided Student's *t*-test); aspartate aminotransferase (AST), as a readout of hepatic and cardiac injury (comparisons were made by two-sided Student's *t*-test); total bilirubin, as a readout of hepatic injury (comparisons were made by Mann–Whitney *U*-test); alkaline phosphatase, as a readout of hepatic and cardiac injury (comparisons were made by Mann–Whitney *U*-test); creatine kinase (CK) and creatinine, as a readout of cardiac and renal injury (comparisons were made by Mann–Whitney *U*-test). All data are mean ± s.d. ($n = 10$ mice). **d**, Immunoblot analysis of p38γ in liver and tumour samples after AAV-Cre infection. Representative western blot of at least three independent experiments. **e**, Number of tumours and tumour size as analysed at the end of the experiment. Data are mean ± s.e.m. $n = 10$ untreated and $n = 20$ cre-treated mice. Comparisons were made by two-sided Student's *t*-test with Welch's correction; $^{*}P < 0.05$; $^{***}P < 0.001$. **f**, Representative contrast-enhanced MRI results from mice 7 months after DEN injection with or without CRE-mediated p38γ deletion. The figure shows axial slices extracted from the 3D volume dataset. Arrowheads mark typical liver tumours. **g**, AAV-Cre-mediated deletion of p38γ protects against streptozotocin-induced HCC. Left, increased liver damage was found after streptozotocin treatment. Comparisons were made by Student's *t*-test; $^{***}P < 0.001$. Right, tumour size as analysed at the end of the experiment. Comparisons were made by one-way ANOVA coupled to Bonferroni's post-test; $^{*}P < 0.05$. Data are mean ± s.e.m. $n = 10$ untreated and $n = 20$ AAV-Cre-treated mice. In the western blots, each lane corresponds to a different mouse.

nature research

Corresponding author(s): Guadalupe Sabio

☐ Initial submission ☐ Revised version ☒ Final submission

Life Sciences Reporting Summary

Nature Research wishes to improve the reproducibility of the work that we publish. This form is intended for publication with all accepted life science papers and provides structure for consistency and transparency in reporting. Every life science submission will use this form; some list items might not apply to an individual manuscript, but all fields must be completed for clarity.

For further information on the points included in this form, see Reporting Life Sciences Research. For further information on Nature Research policies, including our data availability policy, see Authors & Referees and the Editorial Policy Checklist.

Experimental design

1. Sample size

   Describe how sample size was determined.

   To choose the size of the sample we have used the 3R rule to ensure statistical validity and significance with the chosen size.

   CNIC has biostatisticians to help in designing our animal experiments. They use th e most up-
   tdate statistical methods to ensure that the correct number of animals will be empl oyed in each experiment. The number of animals in each group is determined by t he statistical power that is required to detect significant biologically relevant differ ences. A meaningful difference in means can be detected using a t-
   test, assuming normality. We use 8-18 mice per group for at least 80% power for o ne- and two-sided testing.

2. Data exclusions

   Describe any data exclusions.

   Yes, animals that presented disease or had been bitten because fight in the cage w ere excluded.

3. Replication

   Describe whether the experimental findings were reliably reproduced.

   Each experiment was performed at least 3 times to validate its reproducibility and they were suscesfull.

4. Randomization

   Describe how samples/organisms/participants were allocated into experimental groups.

   Yes, the cages are randomly allocated in our animal facility

5. Blinding

   Describe whether the investigators were blinded to group allocation during data collection and/or analysis.

   Yes, technicians were blinded analyzing samples and most of the studies were perf ormed in such condition, except in some experiments (e.g. western blots) where sa mples were needed to be loaded correctly.

Note: all studies involving animals and/or human research participants must disclose whether blinding and randomization were used.

6. Statistical parameters

For all figures and tables that use statistical methods, confirm that the following items are present in relevant figure legends (or in the Methods section if additional space is needed).

n/a	Confirmed
☐	☒ The exact sample size (*n*) for each experimental group/condition, given as a discrete number and unit of measurement (animals, litters, cultures, etc.)
☐	☒ A description of how samples were collected, noting whether measurements were taken from distinct samples or whether the same sample was measured repeatedly
☐	☒ A statement indicating how many times each experiment was replicated
☐	☒ The statistical test(s) used and whether they are one- or two-sided (note: only common tests should be described solely by name; more complex techniques should be described in the Methods section)
☐	☒ A description of any assumptions or corrections, such as an adjustment for multiple comparisons
☐	☒ The test results (e.g. *P* values) given as exact values whenever possible and with confidence intervals noted
☐	☒ A clear description of statistics including central tendency (e.g. median, mean) and variation (e.g. standard deviation, interquartile range)
☐	☒ Clearly defined error bars

See the web collection on statistics for biologists for further resources and guidance.

Software

Policy information about availability of computer code

7. Software

Describe the software used to analyze the data in this study.

GraphPad Prism 5
OsiriX
AMBER 16:

D.A. Case, R.M. Betz, D.S. Cerutti, T.E. Cheatham, III, T.A. Darden, R.E. Duke, T.J. Giese, H. Gohlke, A.W. Goetz, N. Homeyer, S. Izadi, P. Janowski, J. Kaus, A. Kovalenko, T.S. Lee, S. LeGrand, P. Li, C. Lin, T. Luchko, R. Luo, B. Madej, D. Mermelstein, K.M. Merz, G. Monard, H. Nguyen, H.T. Nguyen, I. Omelyan, A. Onufriev, D.R. Roe, A. Roitberg, C. Sagui, C.L. Simmerling, W.M. Botello-Smith, J. Swails, R.C. Walker, J. Wang, R.M. Wolf, X. Wu, L. Xiao and P.A. Kollman (2016), AMBER 2016, University of California, San Francisco

Gaussian 09:

Gaussian 09, Revision D.01, M. J. Frisch, G. W. Trucks, H. B. Schlegel, G. E. Scuseria, M. A. Robb, J. R. Cheeseman, G. Scalmani, V. Barone, G. A. Petersson, H. Nakatsuji, X. Li, M. Caricato, A. Marenich, J. Bloino, B. G. Janesko, R. Gomperts, B. Mennucci, H. P. Hratchian, J. V. Ortiz, A. F. Izmaylov, J. L. Sonnenberg, D. Williams-Young, F. Ding, F. Lipparini, F. Egidi, J. Goings, B. Peng, A. Petrone, T. Henderson, D. Ranasinghe, V. G. Zakrzewski, J. Gao, N. Rega, G. Zheng, W. Liang, M. Hada, M. Ehara, K. Toyota, R. Fukuda, J. Hasegawa, M. Ishida, T. Nakajima, Y. Honda, O. Kitao, H. Nakai, T. Vreven, K. Throssell, J. A. Montgomery, Jr., J. E. Peralta, F. Ogliaro, M. Bearpark, J. J. Heyd, E. Brothers, K. N. Kudin, V. N. Staroverov, T. Keith, R. Kobayashi, J. Normand, K. Raghavachari, A. Rendell, J. C. Burant, S. S. Iyengar, J. Tomasi, M. Cossi, J. M. Millam, M. Klene, C. Adamo, R. Cammi, J. W. Ochterski, R. L. Martin, K. Morokuma, O. Farkas, J. B. Foresman, and D. J. Fox, Gaussian, Inc., Wallingford CT, 2016.

Jalview Version 2—a multiple sequence alignment editor and analysis workbench
Andrew M. Waterhouse James B. Procter David M. A. Martin Michèle ClampGeoffrey J. Barton
Bioinformatics, Volume 25, Issue 9, 1 May 2009, Pages 1189–1191,https://doi.org/10.1093/bioinformatics/btp033

For manuscripts utilizing custom algorithms or software that are central to the paper but not yet described in the published literature, software must be made available to editors and reviewers upon request. We strongly encourage code deposition in a community repository (e.g. GitHub). *Nature Methods* guidance for providing algorithms and software for publication provides further information on this topic.

Materials and reagents

Policy information about availability of materials

8. Materials availability

Indicate whether there are restrictions on availability of unique materials or if these materials are only available for distribution by a for-profit company.	No unique materials were used.

9. Antibodies

Describe the antibodies used and how they were validated for use in the system under study (i.e. assay and species).	All the antibodies used are fully described in the material and methods section (supplier, catalogue number, lote, clone and working dilution). The antibodies were validated prior to their use. Antibodies Dilution Reference 1. Rb (D20) Cell Signaling 1:1000 9313S 2. Rb Sta. Cruz Wb 1:100; IP: 4ug Rb (IF8) sc- 102 3. GAPDH 1:1000 FL-335 sc-25778 4. Tubulin Sigma 1:1000 SIGMA T6199 5. Vinculin Sigma 1:1000 V9131 6. p-Rb S807/811 Cell Signaling 1:1000 8516S 7. p-Rb S795 Cell signaling Wb 1:1000 IHC 1:250 9301S 8. p-Rb S780 Cell signaling 1:1000 8180S 9. p-Rb S608 Cell signaling 1:1000 F4 sc- 377540 10. p-Rb T821/826 Cell signaling 1:1000 E10 sc- 271930 11. p-p38 Cell Signaling 1:1000 (T180/Y182) 9211S 12. p38 gamma Cell Signaling Wb 1:100; IP: 4ug 2307S 13. p38 alpha Sta. Cruz 1:1000 F9 sc- 271120 14. PCNA 1:1000 Ab 18197 15. CDK2 Sta. Cruz Wb 1:1000; IP: 4ug D12 sc- 6248 16. CDK4 Sta. Cruz Wb 1:1000; IP: 4ug C22 sc- 260 17. BrdU (ABCAM) IHC 1:100 Ab 6326 18. Ki67 (ABCAM) IHC 1:100 Ab 16667

10. Eukaryotic cell lines

a. State the source of each eukaryotic cell line used.	Hepatocellular carcinoma cell lines derived from human patients (HepG2, Huh7, Snu354, Snu398 and Snu449, NCBI Biosample) and wild-type human hepatocytes (HepaRG from Life Technologies) were used in the study.
b. Describe the method of cell line authentication used.	Primary hepatocytes were obteined diretly from the company. We verify the cells lines used in this manuscript using microsatellite analysis.
c. Report whether the cell lines were tested for mycoplasma contamination.	Each cell line used in the study were tested for mycoplasma contamination and all of them were negative.
d. If any of the cell lines used are listed in the database of commonly misidentified cell lines maintained by ICLAC, provide a scientific rationale for their use.	No commonly misidentified cell line were used.

Animals and human research participants

Policy information about studies involving animals; when reporting animal research, follow the ARRIVE guidelines

11. Description of research animals

Provide details on animals and/or animal-derived materials used in the study.	We have used male mice C57BL6 from 9 to 16 weeks old depending on the experimental approach.

Policy information about studies involving human research participants

12. Description of human research participants

Describe the covariate-relevant population characteristics of the human research participants.

liver samples from 37 patients (86.1% male, mean age: 69.2 years, standard deviation [SD]: 22.6 years) and 11 controls (36.4% male, mean age: 45.9 years, standard deviation [SD]: 14.7 years) recruited at the University Hospital of Salamanca, Spain. Patients were diagnosed with hepatocellular carcinoma by liver biopsy, and control individuals were recruited from patients who underwent laparoscopic cholecystectomy for gallstone disease and had no laboratory or histopathological evidence of other liver diseases. This study was approved by the Ethics Committee of the University Hospital of Salamanca. A portion of each liver biopsy was fixed in 10% formalin and stained with haematoxylin-eosin and Masson's trichrome for standard histopathological interpretation. Immunostaining of p38γ was performed with an antibody from R&D (AF1347; 1:250).
For the analysis of liver mRNA levels, the study population included 2 groups. One group consisted of obese adult patients with body mass index (BMI) ≥ 35kg/m2 and a liver biopsy compatible with NAFLD who underwent elective bariatric surgery (n= 79). The second group consisted of individuals with BMI < 35kg/m2 who underwent laparoscopic cholecystectomy for cholelithiasis (n= 30).